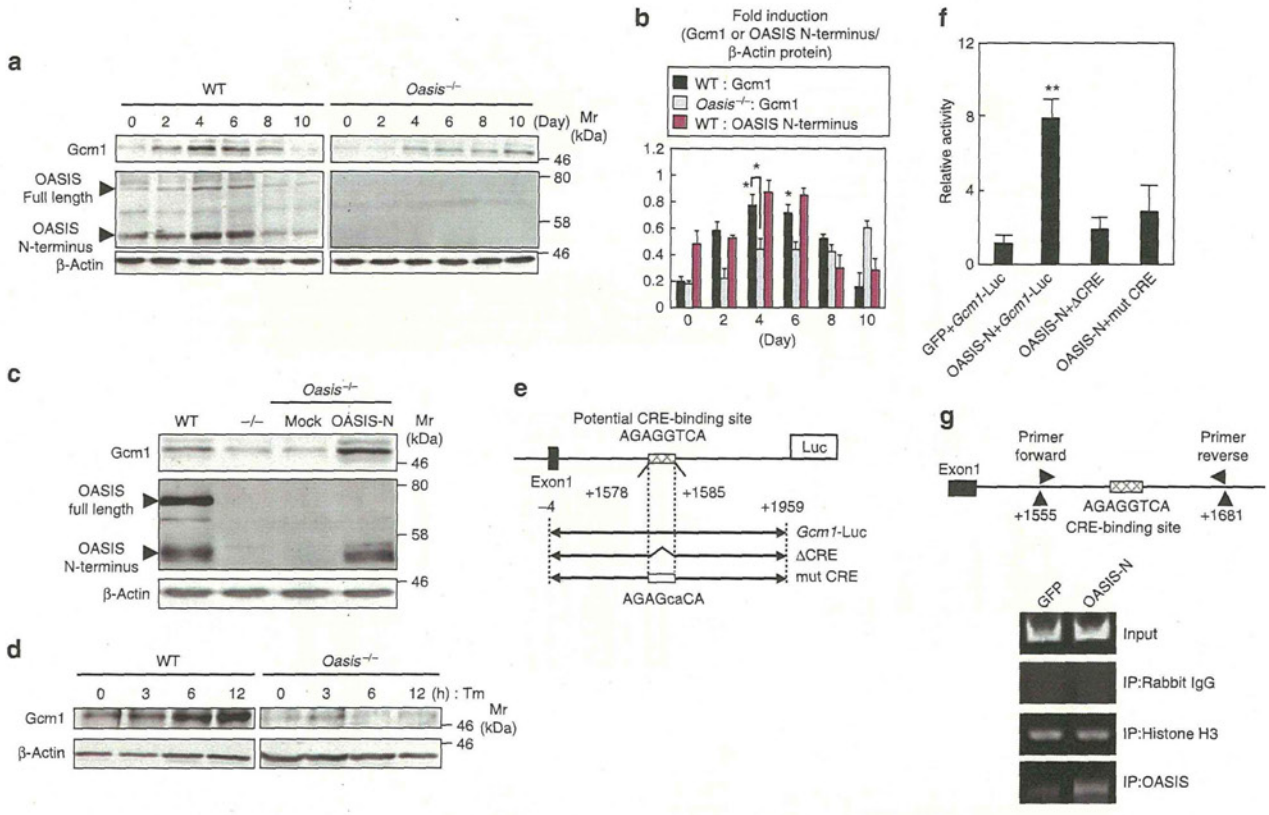

Figure 3 | Gcm1 is a direct target of OASIS in NPCs. (**a**) Western blotting of Gcm1 in NPCs treated with LIF and BMP2 for the indicated times. In WT cells, Gcm1 is transiently upregulated at the same time as OASIS. By contrast, it was significantly downregulated in *Oasis*$^{-/-}$ NPCs. (**b**) Quantitative analysis of expression of Gcm1 and OASIS N-terminus in (**a**). (**c**) Western blotting of Gcm1 using NPCs cultured for 4 days. Adenoviruses expressing OASIS N-terminus were infected with *Oasis*$^{-/-}$ NPCs. Mock indicates empty vector. (**d**) Western blotting of Gcm1 using NPCs treated with LIF and BMP2 for 4 days. Cells were exposed to 3 μg ml^{-1} tunicamycin (Tm; an ER stressor) for the indicated times. (**e**) Scheme of the mouse *Gcm1* promoter region and reporter constructs. The *Gcm1*-Luc construct consists of 2.0 kb from the *Gcm1* promoter region. ΔCRE lacks the CRE-binding site (AGAGGTCA), and mut CRE is mutated (small letters of CRE sequence) in the CRE-binding site. Luc, luciferase gene. (**f**) Reporter assays using NPCs. Vectors expressing the mouse OASIS N-terminus or green fluorescent protein (GFP) were co-transfected with each reporter construct. GFP was used as a control. (**g**) The top panel shows a schematic representation of the *Gcm1* promoter and the annealing sites of the primer set used in the ChIP assays. The bottom panel shows the results of PCR amplification of the *Gcm1* promoter region containing the CRE-binding site (+1,555 to +1,681). NPCs were transfected with the vector expressing the mouse OASIS N-terminus. GFP was used as a control. All bars represent the mean values ±s.d. of three experiments. Significant difference between two samples was determined by unpaired Student's *t*-test (**b**). *P < 0.05, between indicated pairs. Multiple comparisons were made using One way ANOVA followed by Tukey's *post hoc* test. *P < 0.05, **P < 0.01, among WT cells (**b**) and all indicated samples (**f**).

that Gcm1 is involved in the demethylation of promoter regions in specific genes[31]. *Gcm1* might be one of the direct target genes of OASIS in NPCs, and it is possible that OASIS is involved in the regulation of astrocyte differentiation through the expression of Gcm1 followed by the demethylation of the *Gfap* promoter. Therefore, we examined the expression levels of Gcm1 during astrocyte differentiation using primary cultured NPCs. Gcm1 was transiently upregulated during the differentiation of NPCs into astrocytes, and the expression pattern was similar to that of OASIS (Fig. 3a,b). However, Gcm1 was dramatically downregulated to about 50% of the WT level on day 4 in *Oasis*$^{-/-}$ cells. We infected primary cultured *Oasis*$^{-/-}$ NPCs with adenovirus expressing the OASIS N-terminus. Gcm1 expression was markedly upregulated by overexpression of the OASIS N-terminus (Fig. 3c). As OASIS is cleaved in response to ER stress, Gcm1 could be induced in NPCs exposed to ER stress, if Gcm1 is a direct target of OASIS in NPCs. Indeed, the expression level of Gcm1 was upregulated in WT NPCs under the ER stress condition. By contrast, the upregulation of Gcm1 was significantly inhibited in *Oasis*$^{-/-}$ NPCs (Fig. 3d). In the cerebral cortices of *Oasis*$^{-/-}$ mice, Gcm1 expression was downregulated (Supplementary Fig. S3); the findings were consistent with the findings in primary cultured NPCs.

To determine whether OASIS acts on the *Gcm1* promoter and activates transcription of *Gcm1* in NPCs, we performed promoter assays using a reporter gene carrying a 2.0-kb promoter region of *Gcm1* (*Gcm1*-Luc) (Fig. 3e). In NPCs transfected with a *Gcm1*-Luc construct, reporter activities were dramatically induced by expression of the OASIS N-terminus (Fig. 3f). The *Gcm1* promoter includes a cAMP-responsive element (CRE) (+1,585 to +1,592 bp) that OASIS can bind to[10]. We next performed a promoter assay using the reporter constructs ΔCRE, which lacks the CRE-binding site, and mut CRE, which has a mutated CRE-binding site (Fig. 3e). In NPCs transfected with these constructs, reporter activities were markedly reduced, despite expression of the OASIS N-terminus (Fig. 3f). Furthermore, we performed chromatin immunoprecipitation (ChIP) assays and detected a high level of OASIS binding to the endogenous *Gcm1* promoter in primary cultured NPCs transfected with the OASIS N-terminus (Fig. 3g). These results indicate

that OASIS directly acts on the CRE sequence within the *Gcm1* promoter and facilitates its transcription in NPCs.

Mild ER stress and activation of UPR. As shown in Fig. 3a, the levels of full-length OASIS and its N-terminus were increased during astrocyte differentiation. The OASIS N-terminus is produced by the cleavage of full-length OASIS in response to ER stress. It is possible that ER stress occurs during differentiation of NPCs into astrocytes. Therefore, we examined the expression of ER stress-related genes during astrocyte differentiation. *Bip*, *p58^{IPK}* and *Erdj4* were slightly upregulated from day 2 to 6 during differentiation of WT and *Oasis*$^{-/-}$ NPCs into astrocytes (Fig. 4a; Supplementary Fig. S4), indicating that all of signalling pathways from the major three sensors including PKR-like endoplasmic reticulum kinase, ATF6 and inositol-requiring 1, are activated during astrocyte differentiation. Furthermore, the transient upregulation of these genes was synchronized with the expression of the OASIS N-terminus (Fig. 5d), indicating that mild ER stress is transiently induced and that OASIS is activated by this mild ER stress during astrocyte differentiation. Although it is unknown, the roles of each pathway of major ER stress sensors. Next, we examined the roles of mild ER stress in cell fates including differentiation and cell death. To determine the level of ER stress during astrocyte differentiation, we quantified the expression levels of *Erdj4* in NPCs exposed to several doses of dithiothreitol (DTT) or tunicamycin (Tm) (Fig. 4b,c). Consequently, we found that the level of ER stress in NPCs exposed to 125 μM DTT or 90 ng ml^{-1} Tm for 48 h was equal to that during astrocyte differentiation (Fig. 4b,c). This level of ER stress did not induce cell death (Fig. 4d–f), but activated UPR signalling pathways including the OASIS-Gcm1 pathway and promoted astrocyte differentiation after treatment with LIF and BMP2 (Fig. 4g). These results indicate that mild ER stress to a lesser extent than the levels that induce cell death is necessary for astrocyte differentiation.

Gcm1 expression modulation by OASIS family members. ER stress-related CREB/ATF family members have the potential to bind to a CRE-binding site in promoter region and promote its transcription[13,16,40]. Thus, we checked the effects of CREB/ATF family members, including OASIS family members, on a *Gcm1*-Luc reporter. Consequently, we found that CREB4 (Fig. 5a) promotes *Gcm1* reporter activities (Fig. 5b; Supplementary Fig. S5). Furthermore, we detected the binding of CREB4 to endogenous *Gcm1* promoter (Fig. 5c). Thus, not only OASIS but also CREB4 could activate the transcription of *Gcm1*. Two previous reports showed that CREB4 does not bind to the CRE sequence (TGACGTCA)[18,19]. Thus far, CREB/ATF family members are known to bind to the several sequences such as TGACCTCA, TGAGGTCA, TGCCGTCA and TGAAGTCA[41–44]. AGAGGTCA sequence in the *Gcm1* promoter region is not identical to TGACGTCA, which is the most common sequence as CREB/ATF family binding sequence. Therefore, it is possible that the manners of binding of OASIS and CREB4 are different from those of the other CREB/ATF family members. CREB/ATF family members are well known to form homodimers or heterodimers to promote transcription[16,45]. Thus, we examined the synergistic effects of CREB/ATF family members on *Gcm1* promoter activities. In NPCs transfected with a *Gcm1*-Luc construct, reporter activities were dramatically induced by co-expression of OASIS and CREB4 (Fig. 5b), and at the same time, the binding of OASIS to *Gcm1* promoter was also significantly increased (Fig. 5c). Conversely, co-expression of OASIS and Luman, which is also an OASIS family member, resulted in significant downregulation of reporter activities and decreased binding of OASIS to the *Gcm1* promoter (Fig. 5b,c).

We next investigated endogenous expression of and direct interactions among OASIS family members during astrocyte differentiation. Both full-length OASIS and CREB4 and their N-termini were upregulated from day 2 to 6 after treatment of NPCs with LIF and BMP2 (Fig. 5d,e). Further, robust binding of OASIS N-terminus and CREB4 N-terminus was detected on day 4 (Fig. 5f). By contrast, binding of OASIS N-terminus and Luman N-terminus was observed on day 10 (Fig. 5f), suggesting that OASIS and CREB4 form a heterodimer in the early stage of astrocyte differentiation, and that Luman binds to OASIS in the late stage of astrocyte differentiation. Taken together, we concluded that an OASIS-CREB4 heterodimer activates transcription of *Gcm1* during astrocyte differentiation. Conversely, Luman inhibits the formation of the OASIS-CREB4 heterodimer by binding to OASIS and downregulate the transcription of *Gcm1*, followed by terminating differentiation of astrocytes.

OASIS family members and Gcm1 promote astrocyte differentiation. To examine whether OASIS family members and Gcm1 could rescue the delay in astrocyte differentiation observed in *Oasis*$^{-/-}$ NPCs, we introduced these molecules into primary cultured *Oasis*$^{-/-}$ NPCs. The expression levels of Gcm1 were upregulated by the introduction of the OASIS N-terminus, or co-expression of OASIS and CREB4 N-termini. However, introduction of the Luman N-terminus did not affect the expression of Gcm1 (Fig. 6a). Immunocytochemical analysis showed that the number of GFAP-positive cells was increased in NPCs treated with LIF and BMP2 for 4 days (Fig. 6b). Conversely, these cells were decreased in *Oasis*$^{-/-}$ NPCs or *Oasis*$^{-/-}$ NPCs expressing the empty vector (Fig. 6c,d). The decrease in the number of GFAP-positive *Oasis*$^{-/-}$ cells was restored to those of WT cells by introduction of OASIS N-terminus (Fig. 6e,j), CREB4 N-terminus (Fig. 6f,j) or Gcm1 (Fig. 6g,j). The co-expression of OASIS N-terminus and CREB4 N-terminus in *Oasis*$^{-/-}$ NPCs resulted in a greater improvement of the delay in astrocyte differentiation than did expression of OASIS N-terminus or CREB4 N-terminus alone (Fig. 6 h,j). The overexpression of Luman N-terminus in *Oasis*$^{-/-}$ NPCs could not restore the delay (Fig. 6i,j). These data indicate that OASIS-CREB4 heterodimerization followed by the induction of Gcm1 is necessary for accelerating astrocyte differentiation, and conversely, that Luman does not accelerate the differentiation of NPCs into astrocytes.

Gcm1 is involved in demethylation of *Gfap* promoter. As shown in Fig. 2, demethylation of *Gfap* promoter was inhibited in *Oasis*$^{-/-}$ NPCs. To examine the mechanisms responsible for the impaired methylation status of the *Gfap* promoter in *Oasis*$^{-/-}$ NPCs, we performed bisulfite sequencing using the *Gfap* promoter (Fig. 7a,b). In NPCs cultured for 4 days, demethylation in the control was suppressed by transfection with a *Gcm1*-specific short interfering RNA (siRNA) (Fig. 7a,b). In *Oasis*$^{-/-}$ NPCs, demethylation of *Gfap* promoter was also inhibited. The introduction of OASIS N-terminus or Gcm1 into *Oasis*$^{-/-}$ NPCs resulted in restoration of the *Gfap* demethylation status (Fig. 7a,b).

We further examined whether demethylation of *Gfap* promoter by OASIS-Gcm1 signalling induces binding of the Stat3-Smads-p300 complex to the promoter by performing ChIP assays using primary cultured NPCs (Fig. 7c,d). The binding of Stat3 and Smads to the endogenous *Gfap* promoter was inhibited in NPCs transfected with the *Gcm1*-specific siRNA (Fig. 7c,d). In *Oasis*$^{-/-}$ NPCs, binding of Stat3 and Smads was also inhibited. The introduction of the OASIS N-terminus or Gcm1 into *Oasis*$^{-/-}$ NPCs restored the binding of Stat3 and Smads to the *Gfap* promoter to the levels seen in WT cells (Fig. 7c,d). These data suggest that the activation of OASIS-Gcm1 signalling accelerates demethylation of the *Gfap* promoter followed by binding of Stat3-Smads-p300 complex.

Discussion

It has been reported that the epigenetic regulation of the methylation status of the *Gfap* promoter is essential for accelerating differentiation

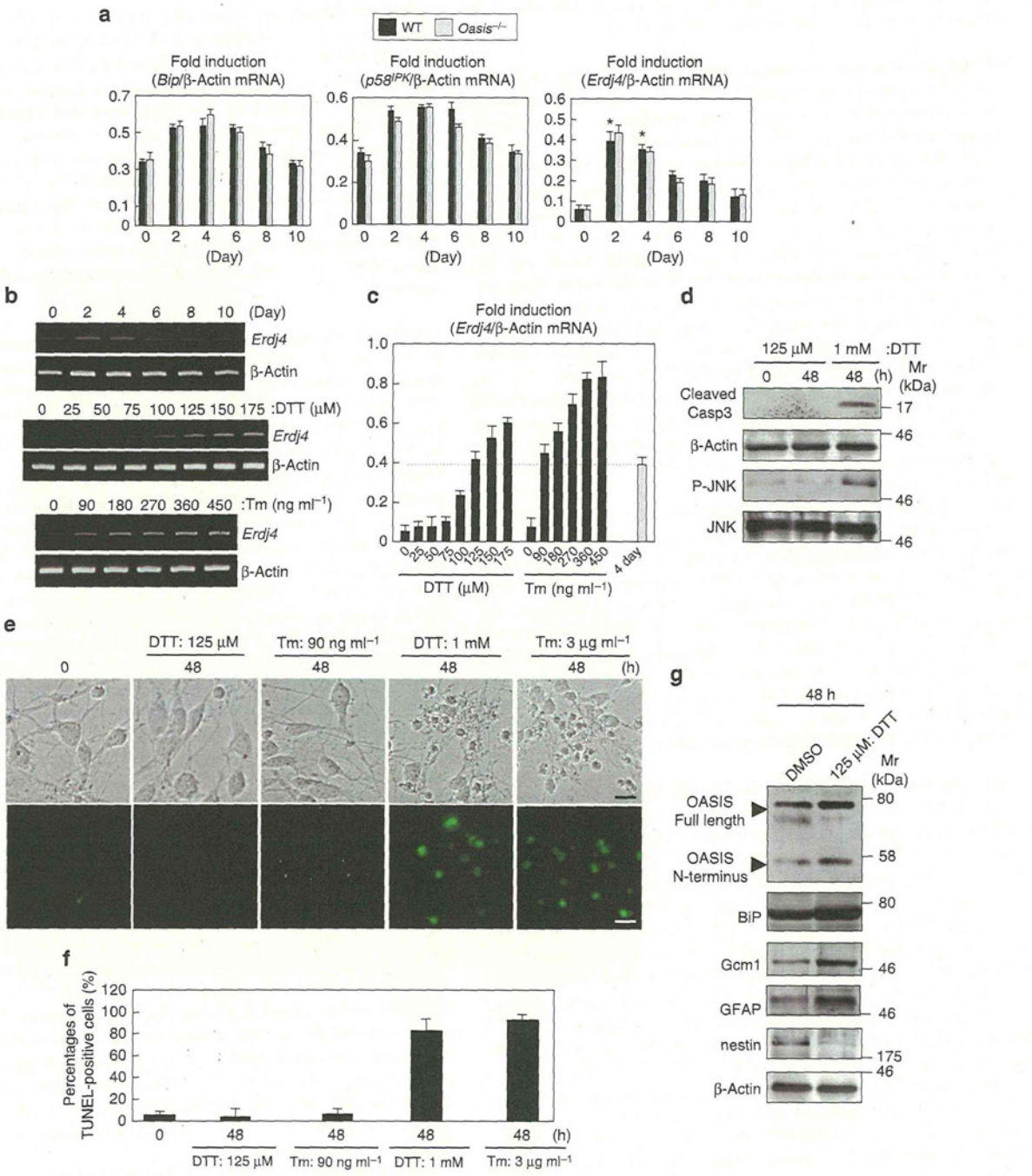

Figure 4 | Mild ER stress promotes astrocyte differentiation. (**a**) Real-time PCR analysis of ER stress-related genes in NPCs treated with LIF and BMP2 for the indicated times. Mild ER stress transiently occurred (from day 2 to day 6) during the differentiation of NPCs into astrocytes. (**b**) RT–PCR analysis of *Erdj4* in NPCs treated with LIF and BMP2 for the indicated times (top panel). Middle and bottom panels show the expression of *Erdj4* in NPCs exposed to DTT (an ER stressor) or Tm for 48 h. (**c**) Quantitative analysis of the expression of *Erdj4* in (**b**). The expression level of *Erdj4* in NPCs treated with LIF and BMP2 for 4 days was very similar to the expression levels in NPCs exposed to 125 μM DTT or 90 ng ml^{-1} Tm for 48 h. The dotted line indicates the expression level of *Erdj4* in NPCs treated with LIF and BMP2 for 4 days. (**d**) Western blotting of cleaved caspase 3 (Casp3) and phosphorylated (P)-JNK in NPCs treated with LIF and BMP2 for 4 days. Cleaved Casp3 and P-JNK were not induced by the same level of mild ER stress observed during astrocyte differentiation. (**e**) Phase contrast images (top panels) and TUNEL staining (bottom panels) in NPCs treated with LIF and BMP2 for 4 days. Cell death was not induced by mild ER stress (125 μM DTT, 90 ng ml^{-1} Tm). Scale bars, 25 μm. (**f**) The percentages of TUNEL-positive cells in (**e**). The number of TUNEL-positive cells was measured in five fields per well. (**g**) Western blotting of OASIS, BiP, Gcm1, GFAP and nestin in NPCs treated with LIF and BMP2 for 4 days. Mild ER stress activated UPR signalling and promoted astrocyte differentiation after treatment with LIF and BMP2. All bars represent the mean values ±s.d. of 4 (**a**,**c**) and 2 (**f**) experiments. Significant difference was determined by One-way ANOVA followed by Tukey's *post hoc* test. $^{*}P<0.05$, among WT cells.

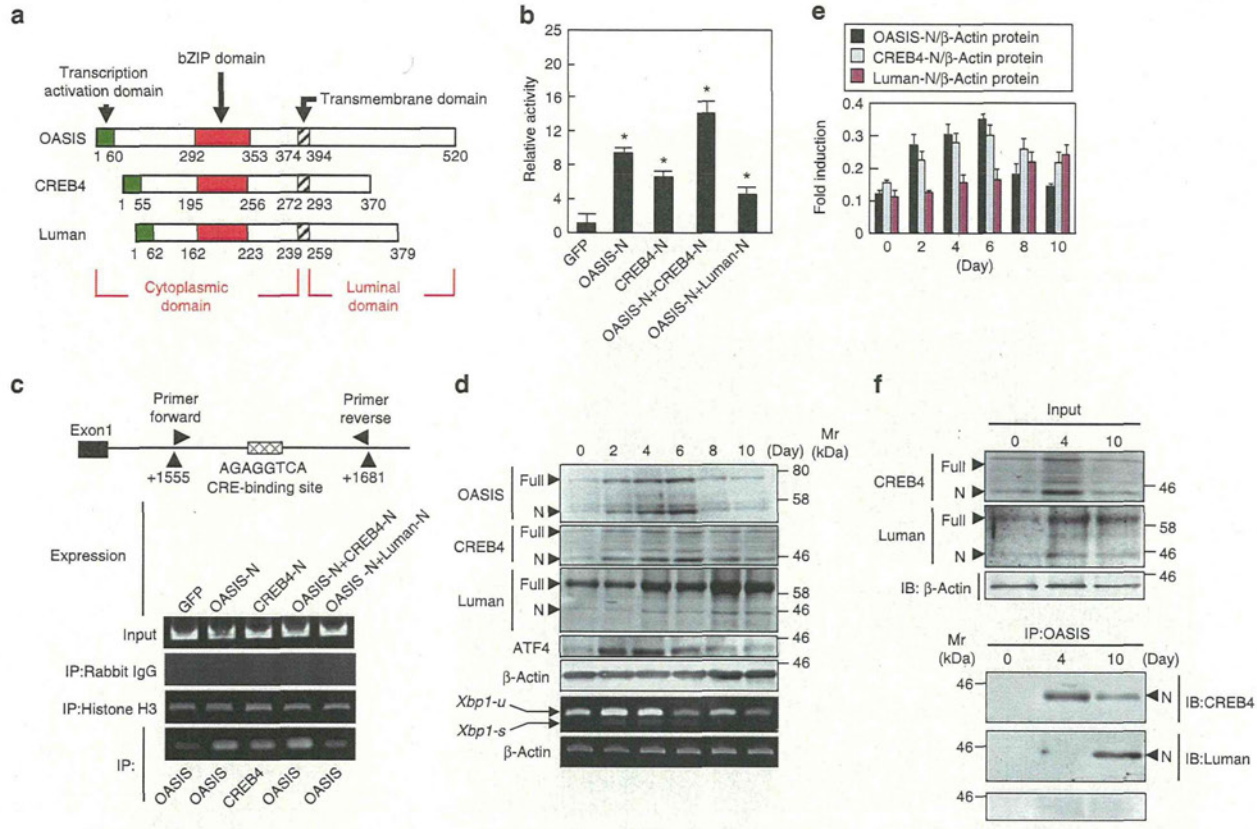

Figure 5 | OASIS and CREB4 form a heterodimer and promote Gcm1 expression. (**a**) Predicted peptide features of mouse OASIS, CREB4 and Luman. (**b**) Reporter assays in NPCs. Expression vectors for the N-terminus of mouse OASIS, CREB4, Luman and GFP were co-transfected with *Gcm1*-Luc. GFP was used as a control. (**c**) The top panel shows a schematic representation of the *Gcm1* promoter and the annealing sites of the primer set used in the ChIP assays. The bottom panel shows the results of PCR amplification of the *Gcm1* promoter region containing the CRE-binding site (+1,555 to +1,681) after immunoprecipitation with indicated antibodies. NPCs were transfected with the expression vectors for the N-terminus of mouse OASIS, CREB4, Luman and GFP. GFP was used as a control. (**d**) Western blotting (OASIS, CREB4, Luman and ATF4) and RT-PCR (*Xbp1*) analysis in NPCs treated with LIF and BMP2 for the indicated times. Both full-length OASIS and CREB4 and their N-termini were upregulated from day 2 to 6 after treatment of NPCs with LIF and BMP2, synchronizing with the transient upregulation of ATF4 and spliced form of *Xbp1* (*Xbp1-s*). Luman N-terminus was upregulated after day 8 in these cells. *Xbp-1-u*: unspliced form of *Xbp1*. (**e**) Quantitative analysis of the expression of N-terminus of OASIS, CREB4 and Luman in (**d**). (**f**) Immunoprecipitation by anti-OASIS antibody followed by western blotting with the indicated antibodies using NPCs treated with LIF and BMP2 for the indicated times. OASIS N-terminus was robustly bound to CREB4 N-terminus on day 4. OASIS, and Luman N-terminus formed a complex on day 10. Input indicates cell lysates before immunoprecipitation. Full, Full length; N, N-terminus; IP, immunoprecipitation; IB, immunoblotting. All bars represent the mean values ±s.d. of three experiments. Significant difference was determined by One-way ANOVA followed by Tukey's *post hoc* test. $^*P<0.05$, among all indicated samples (OASIS-N, CREB4-N and OASIS-N+CREB4-N) or the samples named OASIS-N, OASIS-N+CREB4-N and OASIS-N+Luman-N (OASIS-N+Luman-N).

of NPCs into astrocytes, and that the impairment of demethylation of the *Gfap* promoter disturbs astrocyte differentiation[38]. However, the regulatory mechanisms underlying demethylation of the *Gfap* promoter have remained unclear. In this study, we found that Gcm1, a direct target of OASIS, regulates the methylation status of the *Gfap* promoter followed by accelerating astrocyte differentiation. Interestingly, Gcm1 expression was fine-tuned by the dynamic interaction among OASIS family members that are activated by ER stress, during astrocyte differentiation. Thus, the spatio-temporal control of Gcm1 expression could contribute to production of functional and mature astrocytes. In this context, this report is the first to show that UPR signalling is linked to astrocyte differentiation. It is well known that not only epigenetic regulation but also the activation of Stat3 and Smads is essential for differentiation of NPCs into astrocytes[32,35,37]. However, the activation of these transcription factors was not affected in *Oasis*$^{-/-}$ mice (Fig. 2c,d). These findings strongly suggest that OASIS-Gcm1 signalling specially acts to regulate demethylation of the *Gfap* promoter, during astrocyte differentiation.

We found that *Gcm1* is a target gene of OASIS in the CNS. This conclusion is supported by the fact that (1) *Gcm1* is significantly downregulated in the cerebral cortices and primary cultured NPCs of *Oasis*$^{-/-}$ mice; (2) a CRE-binding site that OASIS can bind to exist in the *Gcm1* promoter region; (3) overexpression of the OASIS N-terminus upregulated *Gcm1* promoter activities; (4) *Gcm1* promoter activities were drastically decreased by mutation or deletion of the CRE-binding site; and (5) OASIS directly binds to the *Gcm1* promoter. *Gcm* homologues have been shown to be involved as master regulators in key steps of differentiation processes[39]. In addition to astrocyte differentiation, Gcm1 is also essential for the differentiation of trophoblasts into syncytiotrophoblasts[39]. The promoter region of *Gcm1* contains several CRE-binding sites containing the OASIS-binding site, we showed in this study. The effects of various

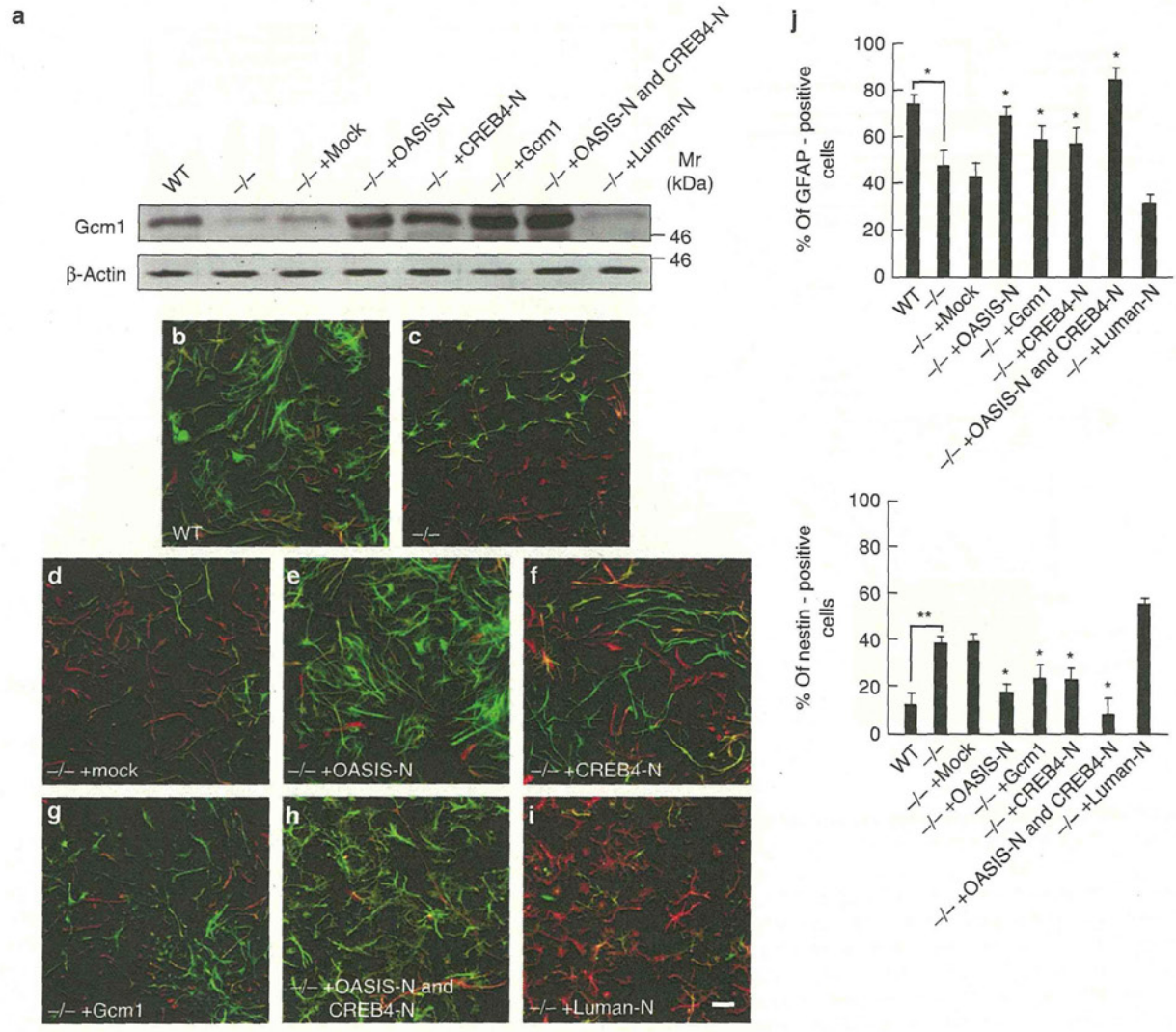

Figure 6 | OASIS family members and Gcm1 rescue the delay in astrocyte differentiation in *Oasis*$^{-/-}$ NPCs. (**a**) Western blotting of Gcm1 in NPCs treated with LIF and BMP2 for 4 days. In *Oasis*$^{-/-}$ NPCs, Gcm1 was upregulated by the introduction of the OASIS N-terminus, the CREB4 N-terminus, or co-expression of both. However, expression of the Luman N-terminus did not affect the expression of Gcm1. Mock indicates empty vector. (**b–i**) Immunostaining of GFAP (green) and nestin (red) in primary cultured NPCs treated with LIF and BMP2 for four days. Mock indicates empty vector. Scale bar, 50 μm. (**j**) The percentages of GFAP- (left panel) and nestin-positive cells (right panel) in (**b–i**). The number of positive cells was measured in five fields per well. All bars represent the mean values ±s.d. of ten experiments. Significant difference between two samples was determined by unpaired Student's *t*-test. $^{*}P<0.05$, $^{**}P<0.01$, between indicated pairs. Multiple comparisons were made using One-way ANOVA followed by Tukey's *post hoc* test. $^{*}P<0.05$, among all indicated samples except for WT.

CREB/ATF transcription factors on the *Gcm1* promoter should be precisely analysed to elucidate the detailed mechanisms underlying cell differentiation regulated by Gcm1.

The mammalian homologues of *gcm* are *Gcm1* and *Gcm2*. These molecules show little homology and have no common functional domains except for the GCM-motif[28]. Previous data have shown that both have the potential to accelerate demethylation of the *Hes5* promoter by direct binding to the GCM-binding site in the promoter followed by acquiring the stem cell properties, but *Gcm2* is a more crucial factor than *Gcm1* for the demethylation of the *Hes5* promoter because of the lower expression of *Hes5* in *Gcm2*$^{-/-}$ mice than in *Gcm1*$^{-/-}$ mice[31]. In our data, expression of *Gcm2* was not changed in *Oasis*$^{-/-}$ mice (data not shown), indicating that *Gcm2* is not associated with the impaired differentiation of astrocytes observed in *Oasis*$^{-/-}$ mice. The expression of *Gcm1* was significantly upregulated in the late stage of mouse embryonic development (Supplementary Fig. S3), whereas that of *Gcm2* was transiently upregulated in the early stage[31]. Therefore, we presume that *Gcm2* is mainly involved in the demethylation of *Hes5* promoter in the early stage of mouse embryonic development, and conversely, that *Gcm1* mainly has a role in the demethylation of the *Gfap* promoter in the late stage. The distinct expression patterns and target promoters for demethylation between *Gcm1* and *Gcm2* may determine glial and neuronal cell lineages, respectively.

We showed that OASIS, CREB4 and Luman activate the UPR signalling in response to mild ER stress, during astrocyte differentiation. Previous studies have shown that UPR signalling activated by mild ER stress is crucial for the differentiation of secretory cells including

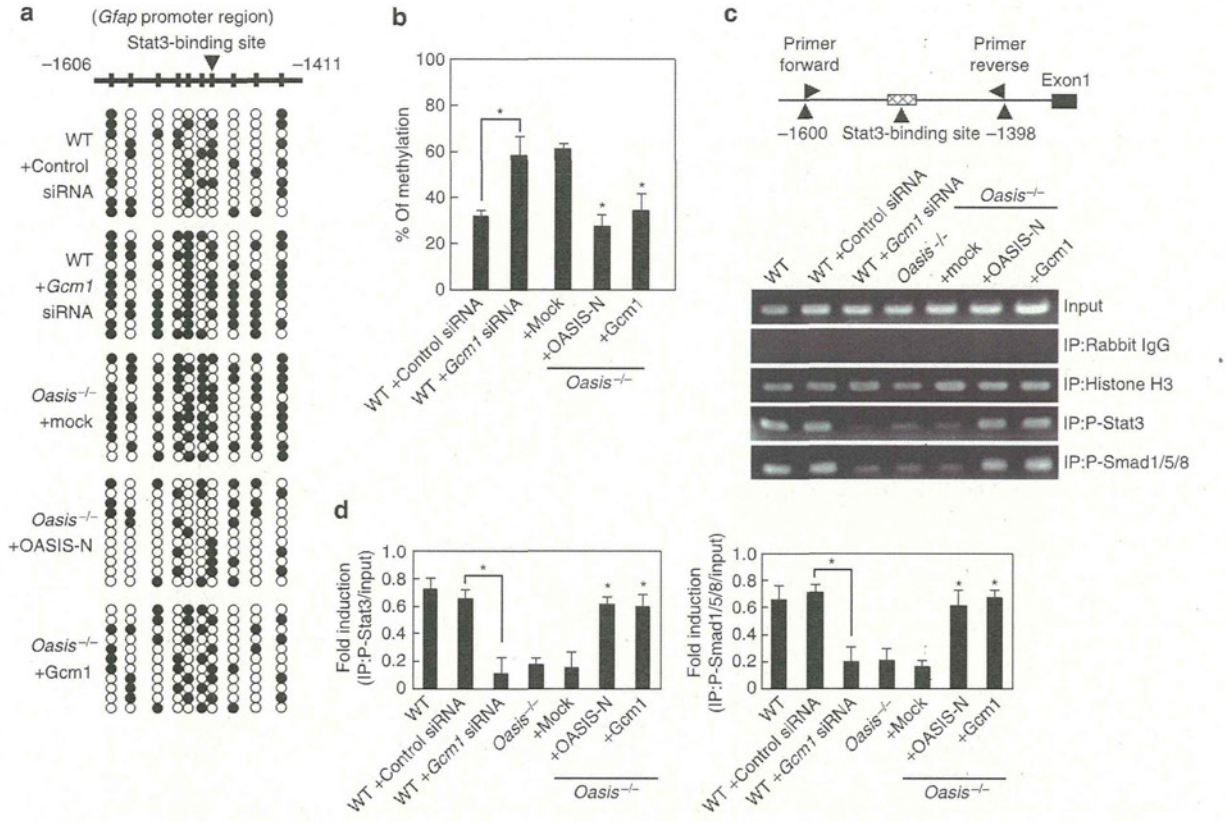

Figure 7 | Gcm1 is involved in demethylation of the *Gfap* promoter. (**a**) Bisulfite sequencing results for the *Gfap* promoter in primary cultured NPCs treated with LIF and BMP2 for four days. (●) and (○) indicate methylated and unmethylated CpG sites, respectively. Experiments were performed using 11 independent samples. Mock indicates empty vector. (**b**) The percentages of methylated sites in the *Gfap* promoter. (**c**) The top panel shows a schematic representation of the *Gfap* promoter and the annealing sites of the primer set used in the ChIP assays. The bottom panel shows the results of PCR amplification of the *Gfap* promoter region containing the Stat3-binding site (−1,398 to −1,600) after immunoprecipitation with the indicated antibodies. Primary cultured NPCs treated with LIF and BMP2 for 4 days were used for ChIP assays. (**d**) Quantitative analysis of PCR amplification after immunoprecipitation by anti-P-Stat3 (top panel) and anti-P-Smad1/5/8 (bottom panel) antibodies in (**c**). All bars represent the mean values ±s.d. of 11 (**b**) and 4 (**d**) experiments. Significant difference between two samples was determined by unpaired Student's *t*-test. $^*P<0.05$, between indicated pairs. Multiple comparisons were made using One-way ANOVA followed by Tukey's *post hoc* test. $^*P<0.05$, among the samples named +mock, +OASIS-N and +Gcm1 (**b**) and *Oasis*−/−, +mock, +OASIS-N and +Gcm1 (**d**).

osteoblasts[21,46–48], chondrocytes[14] and plasma cells[49]. During the differentiation of progenitor cells into these mature secretory cells, secretory materials are gradually produced, and abundant nascent proteins are delivered to the ER. Such an event may serve as a trigger for mild ER stress. Astrocytes also synthesize and secrete various neurotrophic factors and cytokines. During differentiation of NPCs into mature astrocytes, UPR signalling in response to the mild ER stress caused by production of abundant secretory proteins could be activated. Indeed, we found that ER stress-related genes were transiently upregulated during astrocyte differentiation. However, it remains unclear what extent of ER stress is needed for cell differentiation or how such mild ER stress activates only UPR signalling, but does not cause ER stress-induced apoptosis.

The cerebral cortices of *Oasis*$^{-/-}$ mice contained few astrocytes in the embryonic stages, but interestingly, the numbers of astrocytes completely recovered to those in WT mice in adulthood (data not shown). We showed that transfection of NPCs with the CREB4 N-terminus activated the transcription of *Gcm1*. Although the detailed underlying mechanisms are unknown, it is possible that CREB4 has the functional complement to promote astrocyte differentiation in *Oasis*$^{-/-}$ mice in adulthood. It has been reported that one of the aetiologies of psychiatric diseases such as schizophrenia and Rett syndrome is disturbance of the neuronal network caused by a decrease in the number of astrocytes in embryonic and infant stages[50,51]. Although the numbers of astrocytes in the cerebral cortices of *Oasis*$^{-/-}$ mice are normal in adulthood at first glance, a functional disturbance of the CNS may occur in adult *Oasis*$^{-/-}$ mice like in the CNS of such human diseases. It is necessary to perform advanced studies such as precise histological analysis and behavioural tests to clarify the association between OASIS and neuronal diseases.

Methods

Mice. C57BL/6 mice or *Oasis*$^{-/-}$ mice were used in this study. The *Oasis*$^{-/-}$ mice were previously established in our laboratory[21]. In all studies comparing WT and *Oasis*$^{-/-}$ mice, sex-matched littermates derived from the mating of *Oasis*$^{+/-}$ mice were used. The experimental procedures and housing conditions for animals were approved by the Committee of Animal Experimentation, Hiroshima University.

Cell culture, plasmids, transfection and adenovirus. Primary cultured NPCs were cultured as previously described[52]. Briefly, the telencephalons of E14.5 WT and *Oasis*$^{-/-}$ mice were triturated in Hank's balanced salt solution (Invitrogen) by mild pipetting with 1 ml pipette tips (Gilson, Greiner Bio-one). Dissociated cells were cultured in 1.27 g l^{-1} NaHCO3, 25 mg l^{-1} insulin (Sigma), 100 mg l^{-1} apo-transferrin (Sigma), 16 mg l^{-1} putrescin (Sigma), 30 nM sodium selenite (Sigma), 20 nM progesterone (Sigma) in D-MEM-F12 (Gibco), containing

10 ng ml^{-1} basic fibroblast growth factor (Pepro Tech) on culture dishes precoated with poly-ornithine (Sigma) and fibronectin (Sigma) for 4 days. The following day, the cells were stimulated with 50 ng ml^{-1} LIF (Sigma) and 50 ng ml^{-1} BMP2 (Sigma) to initiate astrocyte differentiation. For knockdown of *Gcm1*, NPCs were transfected with a Gcm1-targeting siRNA (Ambion; 4390771) or a non-targeting siRNA (Thermo Scientific; D-001206-13-05) as a control using Lipofectamine 2000 reagent (Invitrogen). Complementary DNAs encoding the N-termini of mouse OASIS, BBF2H7, ATF6, Luman, CREBH and CREB4, the spliced form of XBP1, and full-length ATF4 were inserted into pCDNA3.1+ (Invitrogen). The complementary DNA sequences are summarized in Supplementary Table S1. Cells were transfected with each expression plasmid using Lipofectamine 2000 reagent. The recombinant adenovirus carrying mouse OASIS was generated previously[21]. Adenovirus vectors expressing the mouse Gcm1 were constructed using the AdenoX Expression system (Clontech), according to the manufacturer's protocol.

Immunohistochemistry. Cerebral cortices of WT and *Oasis*$^{-/-}$ mice at the indicated stages were fixed in 4% paraformaldehyde (PFA). Samples were then dehydrated with ethanol, embedded in paraffin and sectioned (5 μm). Paraffin sections were stained with antibodies and visualized under a fluorescence microscope (BX51, Olympus) or a confocal microscope (FV1000D, Olympus). The following antibodies and dilutions were used: anti-GFAP (Sigma; 1:200), and anti-nestin (Abcam; 1:200). The anti-OASIS monoclonal antibody (1:500) was generated previously[21].

***In situ* hybridization**. *In situ* hybridization was performed using digoxigenin-labelled *Oasis* antisense RNA (cRNA) probes[21]. *Oasis* cRNA probes were made by *in vitro* transcription in the presence of digoxigenin-labelled dUTP, using *Oasis* cRNA subcloned into the pGEM-Teasy vector (Promega) as templates. Cerebral cortices were frozen immediately and sectioned (5 μm). Frozen sections were fixed for 20 min with 4% formalin. Then the sections were treated with 0.1% proteinase K for 5 min. After washing with PBS, the sections were re-fixed for 20 min with 4% formalin, and treated with 0.1 M triethanolamine, 2.5% anhydrous acetic acid for 10 min. Sections were prehybridized for 1 h at 37 °C in hybridization buffer (0.01% dextran sulfate, 0.01 M Tris–HCl pH 8.0, 0.05 M NaCl, 50% formamide, 0.2% sarcosyl, 1× Denhardt's solution, 0.5 mg ml^{-1} yeast tRNA, 0.2 mg ml^{-1} salmon testis DNA), and hybridized overnight at 55 °C. After washing with 4×saline sodium citrate buffer for 20 min at 60 °C followed by 2×saline sodium citrate buffer, 50% formamide for 30 min at 60 °C, sections were treated with RNaseA in RNase buffer (10 mM Tris–HCl pH 7.4, 1 mM 0.5 M EDTA (pH 8.0), 0.5 M NaCl) for 30 min at 37 °C to remove un-hybridized probe. After RNase treatment, sections were washed with 2×saline sodium citrate buffer, 50% formamide for 30 min at 60 °C, and then blocked with 1.5% blocking reagent in 100 mM Tris–HCl pH 7.5, 150 mM NaCl for 60 min at room temperature. For detection of digoxigenin-labelled cRNA probes, anti-digoxigenin antibody conjugated to alkaline phosphatase (Roche) was used at a dilution of 1:500, and colour was developed by incubation with 4-nitro blue tetrazolium chloride and 5-bromo-4-chloro-3-indolyl phosphate solution.

Quantitative real-time PCR and RT–PCR. Total RNA was isolated using an RNeasy kit (Qiagen) according to the manufacturer's protocol. First-strand cDNA was synthesized in a 20-μl reaction volume using random primers (Takara) and Moloney murine leukemia virus reverse transcriptase (Invitrogen). Quantitative real-time PCR reactions were performed using a Light Cycler 480 system II (Roche) and Light Cycler SYBR Green I Master (Roche). RT–PCR was performed using each specific primer set in a total volume of 30 μl containing 0.8 μM of each primer, 0.2 mM dNTPs, 3 units of Taq polymerase, and 10×PCR buffer (Agilent). The density of each band on RT–PCR was quantified using Photoshop Elements 2.0 (Adobe Systems). Primer sequences are summarized in Supplementary Table S2.

Western blotting. Proteins were extracted from cells or mice cerebral cortices using cell extraction buffer containing 2.5 mM methionine, 33.3 mM Tris-acetate pH 8.5, 5 mM EDTA, 0.3% SDS, 1.5% Triton, and protease inhibitor cocktail (MBL). Lysates were incubated on ice for 45 min. After centrifugation at 15,000 *g* for 15 min, the soluble protein concentration was measured using BCA protein assay reagents (Pierce). The following antibodies and dilutions were used: anti-β-actin (Sigma; 1:3,000), anti-GFAP (Sigma; 1:1,000), anti-S100β (Abcam; 1:1,000), anti-nestin (Abcam; 1:500), anti-brain lipid-binding protein (Abcam; 1:500), anti-NeuN (CHEMICON; 1:1,000), anti-GSTπ (BD Transduction Laboratories; 1:1,000), anti-phosphorylated-Stat3 (Santa Cruz Biotechnology; 1:500), anti-phosphorylated-Smad1/5/8 (Cell Signaling; 1:1,000), anti-Gcm1 (Santa Cruz Biotechnology; 1:500), anti-Luman (Santa Cruz Biotechnology; 1:250), anti-ATF4 (Santa Cruz Biotechnology; 1:500), anti-ATF6 (Santa Cruz Biotechnology; 1:250), anti-JNK (Cell Signaling; 1:1,000), anti-phosphorylated-JNK (Cell Signaling; 1:1,000), anti-Caspase 3 (Cell Signaling; 1:1,000), anti-BiP (MBL; 1:1,000), and anti-XBP1 (Santa Cruz Biotechnology; 1:250). The anti-OASIS monoclonal antibody (1:1,000) was generated previously[21]. The anti-CREB4 polyclonal antibody (1:1,000) was generated by immunizing mice against mouse recombinant CREB4 (amino acids 1–162). The density of each band was quantified using Photoshop Elements 2.0 (Adobe Systems).

Immunofluorescence. Cells were fixed in 4% PFA and then permeabilized in 0.5% Triton-X 100. The following antibodies and dilutions were used: anti-GFAP (Sigma; 1:500), and anti-nestin (Abcam; 1:250). Cells were visualized under a fluorescence microscope or a confocal microscope (FV1000D, Olympus). The number of positive cells was measured in five fields per well.

TUNEL assay. Primary cultured NPCs prepared from E14.5 WT and *Oasis*$^{-/-}$ mice were fixed in 4% PFA and then permeabilized in 0.1% sodium citrate and 0.1% Triton-X 100. TdT-mediated dUTP nick end labeling (TUNEL) staining was performed using the Cell Death Detection kit, Fluorescein (Roche), according to the manufacturer's protocol. Cells were visualized under a fluorescence microscope. The number of positive cells was measured in five fields per well.

Immunoprecipitation assay. Cells were washed with PBS and lysed with 1 ml of 1% CHAPSO (Sigma) buffer. Cell lysates were centrifuged at 15,000*g* at 4 °C for 15 min and supernatants collected and then incubated with anti-OASIS antibody overnight. Then, samples were incubated with protein G–Sepharose beads (GE Healthcare Life Sciences) for an additional 2 h at 4 °C. Beads were washed with TNE buffer, containing 10 mM Tris, 1 mM EDTA and 150 mM NaCl. Subsequently, samples were subjected to western blotting with anti-CREB4 or anti-Luman antibody.

Luciferase assay. Primary cultured NPCs prepared from E14.5 WT and *Oasis*$^{-/-}$ mice were cultured for 4 days and transfected with 0.2 μg of a pGL3 basic reporter plasmid carrying the firefly luciferase gene (Promega) and 0.02 μg of the reference plasmid pRL-SV40 carrying the Renilla luciferase gene under the control of the SV40 enhancer and promoter (Promega), together with 0.2 μg of an effector protein expression plasmid, using Lipofectamine 2000 reagent. UPRE-LUC reporter was kind gift from Ron Prywes (Columbia University)[53]. After 24 h, luciferase activities were measured using the Dual-Luciferase Reporter Assay System (Promega) and a luminometer (Berthold Technologies), according to the manufacturer's protocol. Relative activity was defined as the ratio of firefly luciferase activity to that of Renilla luciferase.

Chromatin immunoprecipitation assay. The chromatin immunoprecipitation assay was performed as previously described[10]. The primers used for the mouse *Gcm1* promoter were: 5′-GAAAAATTATTAACATGTGTGAATGCAT-3′ (forward) and 5′-CTCAAAAGAGGGTGGTGGGGGGCTTA-3′ (reverse) yielding a 127-bp product. Those used for the mouse *Gfap* promoter were: 5′-CCTTCCC TATGGTGGGACTCATTAGGAG-3′ (forward) and 5′-CATGCTTGGGCTTC TGGTGTCTACTCCAG-3′ (reverse) yielding a 209-bp product. The following antibodies were used: anti-OASIS[21], anti-CREB4 (generated by immunizing mice against mouse recombinant CREB4: amino acids 1–162), anti-histone H3 (Santa Cruz Biotechnology), and rabbit IgG (Sigma).

Bisulfite sequencing. Procedures were performed as previously described[52]. Sodium bisulfite treatment of genomic DNA was performed using a Methylamp DNA Modification kit (Epigentek), according to the manufacturer's protocol. The region in the *Gfap* promoter containing the Stat-binding site of the bisulfite-treated genomic DNA was amplified by PCR using the following primers: 5′-GGGATTT ATTAGGAGAATTTTAGAAGTAG-3′ (forward) and 5′-TCTACCCATACTTAAA CTTCTAATATCTAC-3′ (reverse). The PCR products were cloned into pCR–Blunt II-TOPO vector (Invitrogen) and at least 11 randomly selected clones were sequenced.

Statistical analysis. Statistical comparisons were made using the unpaired Student's-*t*-test (between two samples) and One-way ANOVA followed by Tukey's *post hoc* test (among multiple samples). The statistical significance of a difference between each sample was determined on the basis of a *P*-value <0.05. *P*-values of <0.05, 0.01 or 0.001 are described as $^{*}P<0.05$, $^{**}P<0.01$, or $^{***}P<0.001$, respectively.

References

1. Ron, D. Translational control in the endoplasmic reticulum stress response. *J. Clin. Invest.* **110,** 1383–1388 (2002).
2. Kaufman, R. J. Orchestrating the unfolded protein response in health and disease. *J. Clin. Invest.* **101,** 1389–1398 (2002).
3. Harding, H. P., Zhang, Y. & Ron, D. Protein translation and folding are coupled by an endoplasmic-reticulum-resident kinase. *Nature* **397,** 271–274 (1999).
4. Tirasophon, W., Welihinda, A. A. & Kaufman, R. J. A stress response pathway from the endoplasmic reticulum to the nucleus requires a novel bifunctional protein kinase/endoribonuclease (Ire1p) in mammalian cells. *Genes Dev.* **12,** 1812–1824 (1998).
5. Calfon, M. *et al.* IRE1 couples endoplasmic reticulum load to secretory capacity by processing the XBP-1 mRNA. *Nature* **415,** 92–96 (2002).
6. Yoshida, H. *et al.* ATF6 activated by proteolysis binds in the presence of NF-Y (CBF) directly to the cis-acting element responsible for the mammalian unfolded protein response. *Mol. Cell. Biol.* **20,** 6755–6767 (2000).

7. Shen, J., Chen, X., Hendershot, L. & Prywes, R. ER stress regulation of ATF6 localization by dissociation of BiP/GRP78 binding and unmasking of Golgi localization signals. *Dev. Cell* **3,** 99–111 (2002).
8. Kondo, S., Saito, A., Asada, R., Kanemoto, S. & Imaizumi, K. Physiological unfolded protein response regulated by CREB/ATF family members, transmembrane bZIP transcription factors. *IUBMB Life* **63,** 233–239 (2011).
9. Asada, R., Kanemoto, S., Kondo, S., Saito, A. & Imaizumi, K. The signaling from endoplasmic reticulum-resident bZIP transcription factors involved in diverse cellullar physiology. *J. Biochem.* **149,** 507–518 (2011).
10. Kondo, S. *et al.* OASIS, a CREB/ATF-family member, modulates UPR signalling in astrocytes. *Nat. Cell Biol.* **7,** 186–194 (2005).
11. Murakami, T. *et al.* Cleavage of the membrane-bound transcription factor OASIS in response to endoplasmic reticulum stress. *J. Neurochem.* **96,** 1090–1100 (2006).
12. Saito, A., Hino, S- I., Murakami, T., Kondo, S. & Imaizumi, K. A novel ER stress transducer, OASIS, expressed in astrocytes. *Antioxid. Redox Signal.* **9,** 563–571 (2007).
13. Kondo, S. *et al.* BBF2H7, a novel transmembrane bZIP transcription factor, is a new type of endoplasmic reticulum stress transducer. *Mol. Cell. Biol.* **27,** 1716–1729 (2007).
14. Saito, A. *et al.* Regulation of endoplasmic reticulum stress response by a BBF2H7-mediated Sec23a pathway is essential for chondrogenesis. *Nat. Cell Biol.* **11,** 1197–1204 (2009).
15. Omori, Y. *et al.* CREB-H: a novel mammalian transcription factor belonging to the CREB/ATF family and functioning via the box-B element with a liver-specific expression. *Nucleic Acids Res.* **29,** 2154–2162 (2001).
16. Zhang, K. *et al.* Endoplasmic reticulum stress activates cleavage of CREBH to induce a systemic inflammatory response. *Cell* **124,** 587–599 (2006).
17. Adham, I. M. *et al.* Reduction of spermatogenesis but not fertility in Creb3l4-deficient mice. *Mol. Cell. Biol.* **25,** 7657–7664 (2005).
18. Stelzer, G. & Don, J. Atce1: a novel mouse cyclic adenosine 3′,5′-monophosphate-responsive element-binding protein- like gene exclusively expressed in postmeiotic spermatids. *Endocrinology* **143,** 1578–1588 (2002).
19. Nagamori, I. *et al.* The testes-specific bZip type transcription factor Tisp40 plays a role in ER stress responses and chromatin packaging during spermiogenesis. *Genes Cells* **11,** 1161–1171 (2006).
20. Lu, R., Yang, P., O'Hare, P. & Misra, V. Luman, a new member of the CREB/ATF family, binds to herpes simplex virus VP16-associated host cellular factor. *Mol. Cell. Biol.* **17,** 5117–5126 (1997).
21. Murakami, T. *et al.* Signalling mediated by the endoplasmic reticulum stress transducer OASIS is involved in bone formation. *Nat. Cell Biol.* **11,** 1205–1211 (2009).
22. Chihara, K. *et al.* Increased vulnerability of hippocampal pyramidal neurons to the toxicity of kainic acid in OASIS-deficient mice. *J. Neurochem.* **110,** 956–965 (2009).
23. Hosoya, T., Takizawa, K., Nitta, K. & Hotta, Y. Glial cells missing: a binary switch between neuronal and glial determination in Drosophila. *Cell* **82,** 1025–1036 (1995).
24. Jones, B. W., Fetter, R. D., Tear, G. & Goodman, C. S. Glial cells missing: a genetic switch that controls glial versus neuronal fate. *Cell* **82,** 1013–1023 (1995).
25. Vincent, S., Vonesch, J. L. & Giangrande, A. Glide directs glial fate commitment and cell fate switch between neurones and glia. *Development* **122,** 131–139 (1996).
26. Takizawa, K. & Hotta, Y. Pathfinding analysis in a glia-less gcm mutant in Drosophila. *Dev. Genes Evol.* **211,** 30–36 (2001).
27. Kim, J. *et al.* Isolation and characterization of mammalian homologs of the Drosophila gene glial cells missing. *Development* **95,** 12364–12369 (1998).
28. Akiyama, Y., Hosoya, T., Poole, A. M. & Hotta, Y. The gcm-motif: a novel DNA-binding motif conserved in *Drosophila* and mammals. *Proc. Natl Acad. Sci. USA* **93,** 14912–14916 (1996).
29. Egger, B. *et al.* Gliogenesis in Drosophila: genome-wide analysis of downstream genes of glial cells missing in the embryonic nervous system. *Development* **129,** 3295–3309 (2002).
30. Iwasaki, Y. *et al.* The potential to induce glial differentiation is conserved between Drosophila and mammalian glial cells missing genes. *Development* **130,** 6027–6035 (2003).
31. Hitoshi, S. *et al.* Mammalian *Gcm* genes induce *Hes5* expression by active DNA demethylation and induce neural stem cells. *Nat. Neurosci.* **14,** 957–964 (2011).
32. Nakashima, K. *et al.* Synergistic signaling in fetal brain by STAT3-Smad1 complex bridged by p300. *Science* **284,** 479–482 (1999).
33. Bonni, A. *et al.* Regulation of gliagenesis in the central nervous system by JAK-STAT signaling pathway. *Science* **278,** 477–483 (1997).
34. Koblar, S. A. *et al.* Neural precursor differentiation into astrocytes requires signaling through the leukemia inhibitory factor receptor. *Proc. Natl Acad. Sci. USA* **95,** 3178–3181 (1998).
35. Nakashima, K. *et al.* Developmental requirement of gp130 signaling in neuronal survival and astrocyte differentiation. *J. Neurosci.* **19,** 5429–5434 (1999).
36. He, F. *et al.* A positive autoregulatory loop of Jak-STAT signaling controls the onset of astrogliagenesis. *Nat. Neurosci.* **8,** 616–625 (2005).
37. Rajan, P. & Mckay, R. D. Multiple routes to astrocytic differentiation in the CNS. *J. Neurosci.* **18,** 3620–3629 (1998).
38. Takizawa, T. *et al.* DNA methylation is a critical cell-intrinsic determinant of astrocyte differentiation in the fetal brain. *Dev. Cell* **1,** 749–758 (2001).
39. Schubert, S. W. *et al.* bZIP-Type transcription factors CREB and OASIS bind and stimulate the promoter of the mammalian transcription factor GCMa/Gcm1 in trophoblast cells. *Nucleic Acids Res.* **36,** 3834–3846 (2008).
40. Clauss, I. M., Chu, M., Zhao, J. L. & Glimcher, L. H. The basic domain/leucine zipper protein hXBP-1 preferentially binds to and transactivates CRE-like sequences containing an ACGT core. *Nucleic Acids Res.* **24,** 1855–1864 (1996).
41. Harris, M. *et al.* Transcriptional regulation of the thyrotropin-releasing hormone gene by leptin and melanocortin signaling. *J. Clin. Invest.* **107,** 111–120 (2001).
42. Berhane, K. & Boggaram, V. Identification of a novel DNA regulatory element in the rabbit surfactant protein B (SP-B) promoter that is a target for ATF/CREB and AP-1 transcription factors. *Gene* **268,** 141–151 (2001).
43. Cote-Vélez, A. *et al.* Dexamethasone represses cAMP rapid upregulation of TRH gene transcription: identification of a composite glucocorticoid response element and a cAMP response element in TRH promoter. *J. Mol. Endocrinol.* **34,** 177–197 (2005).
44. Sheng, Z. *et al.* A genome-wide RNA interference screen reveals an essential CREB3L2-ATF5-MCL1 survival pathway in malignant glioma with therapeutic implications. *Nat. Med.* **16,** 671–677 (2010).
45. Hai, T. & Hartman, M. G. The molecular biology and nomenclature of the activating transcription factor/cAMP responsive element binding family of transcription factors: activating transcription factor proteins and homeostasis. *Gene* **273,** 1–11 (2001).
46. Wei, J., Sheng, X., Feng, D., McGrath, B. & Cavener, D. R. PERK is essential for neonatal skeletal development to regulate osteoblast proliferation and differentiation. *J. Cell Physiol.* **217,** 693–707 (2008).
47. Saito, A. *et al.* Endoplasmic reticulum stress response mediated by the PERK-eIF2á-ATF4 pathway is involved in osteoblasts differentiation induced by BMP2. *J. Biol. Chem.* **286,** 4809–4818 (2011).
48. Tohmonda, T. *et al.* The IRE1á-XBP1 pathway is essential for osteoblasts differentiation through promoting transcription of *Osterix*. *EMBO Rep.* **12,** 451–457 (2011).
49. Gass, J. N., Gifford, N. M. & Brewer, J. W. Activation of an unfolded protein response during differentiation of antibody-secreting B cells. *J. Biol. Chem.* **277,** 49047–49054 (2002).
50. Cotter, D. R., Pariante, C. M. & Everall, I. P. Glial cell abnormalities in major psychiatric disorders: the evidence and implications. *Brain Res. Bull.* **55,** 585–595 (2001).
51. Nagai, K., Miyake, K. & Kubota, T. A transcriptional repressor MeCP2 causing Rett syndrome is expressed in embryonic non-neuronal cells and controls their growth. *Dev. Brain Res.* **157,** 103–106 (2005).
52. Sanosaka, T. *et al.* Identification of genes that restrict astrocyte differentiation of midgestational neural precursor cells. *Neuroscience* **155,** 780–788 (2008).
53. Wang, Y. *et al.* Activation of ATF6 and an ATF6 DNA binding site by the endoplasmic reticulum stress response. *J. Biol. Chem.* **275,** 27013–27020 (2000).

Acknowledgements

We thank M. Tohyama and S. Shiosaka for helpful discussions and critical reading of the manuscript. We also thank S. Nakagawa, K. Takedachi, and M. Harada for technical support. This work was partly supported by grants from the Japan Society for the Promotion of Science KAKENHI (#22020030, #22800049), Sumitomo Foundation, Mochida Memorial Foundation for Medical and Pharmaceutical Research, Astellas Foundation for Research on Metabolic Disorders, Takeda Science Foundation, The Pharmacological Research Foundation Tokyo, Daiichi-Sankyo Foundation of Life Science, The Naito Foundation, Senri Life Science Foundation, Hokuto Foundation for Bioscience, and The Japan Prize Foundation.

Author contributions

A.S. and K.I. designed the experiments. A.S., S.K., N.K., R.A., H.I., M.O., H.M. and S.I. performed the experiments. T.S. and K.N guided the experiments of astrocyte differentiation. T.S. and K.N. provided substantial input into the writing of the manuscript. A.S. and K.I. wrote the manuscript. K.I. supervised the project.

Additional information

Supplementary Information accompanies this paper at http://www.nature.com/naturecommunications

Competing financial interests: The authors declare no competing financial interests.

Reprints and permission information is available online at http://npg.nature.com/reprintsandpermissions/

How to cite this article: Saito, A. *et al.* Unfolded protein response, activated by OASIS family transcription factors, promotes astrocyte differentiation. *Nat. Commun.* 3:967 doi: 10.1038/ncomms1971 (2012).

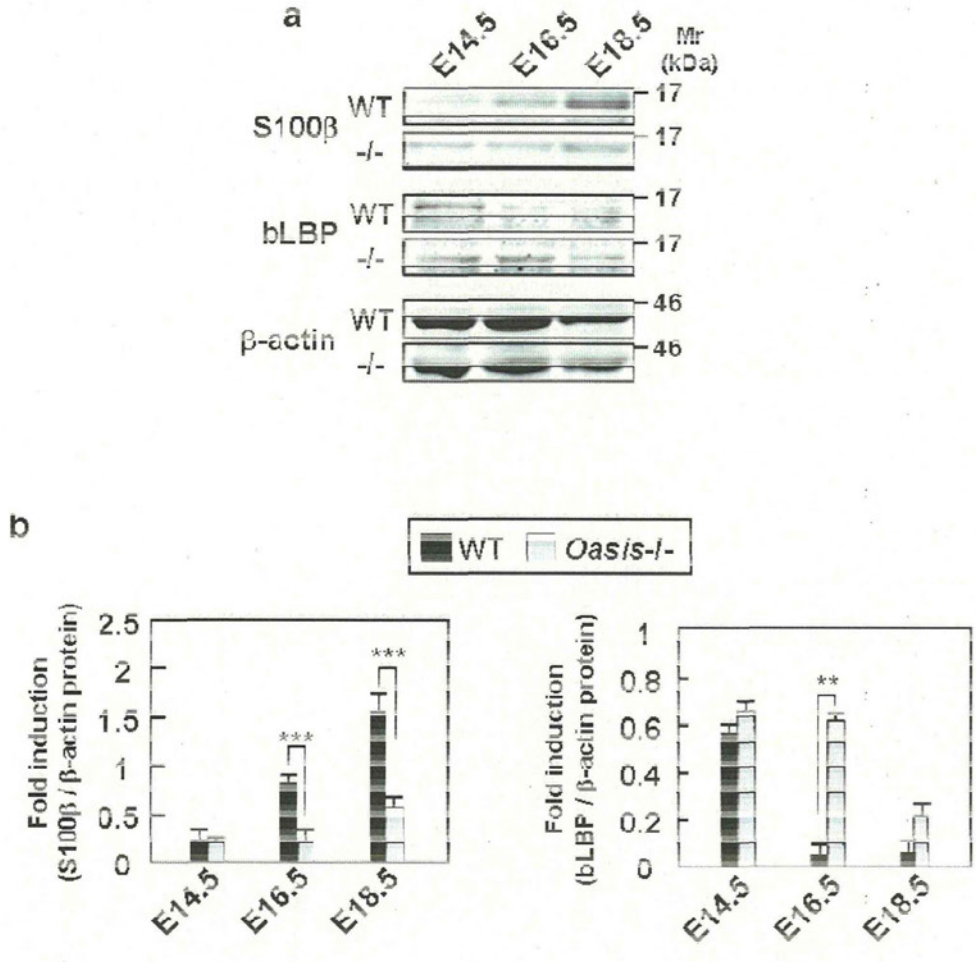

Supplementary Figure S1. Cerebral cortices of *Oasis*$^{-/-}$ in the embryonic stage. (**a**) Western blotting of S100β and bLBP in the cerebral cortices of wild-type (WT) and *Oasis*$^{-/-}$ mice. The expression levels of S100β were markedly lower, and those of bLBP were higher, in the cerebral cortices of *Oasis*$^{-/-}$ mice. (**b**) Quantitative analysis of protein expression levels in (**a**). All bars represent the mean values ±s.d. of 3 experiments. Significant difference was determined by unpaired Student's-*t*-test. $^{**}P < 0.01$, $^{***}P < 0.001$, between indicated pairs.

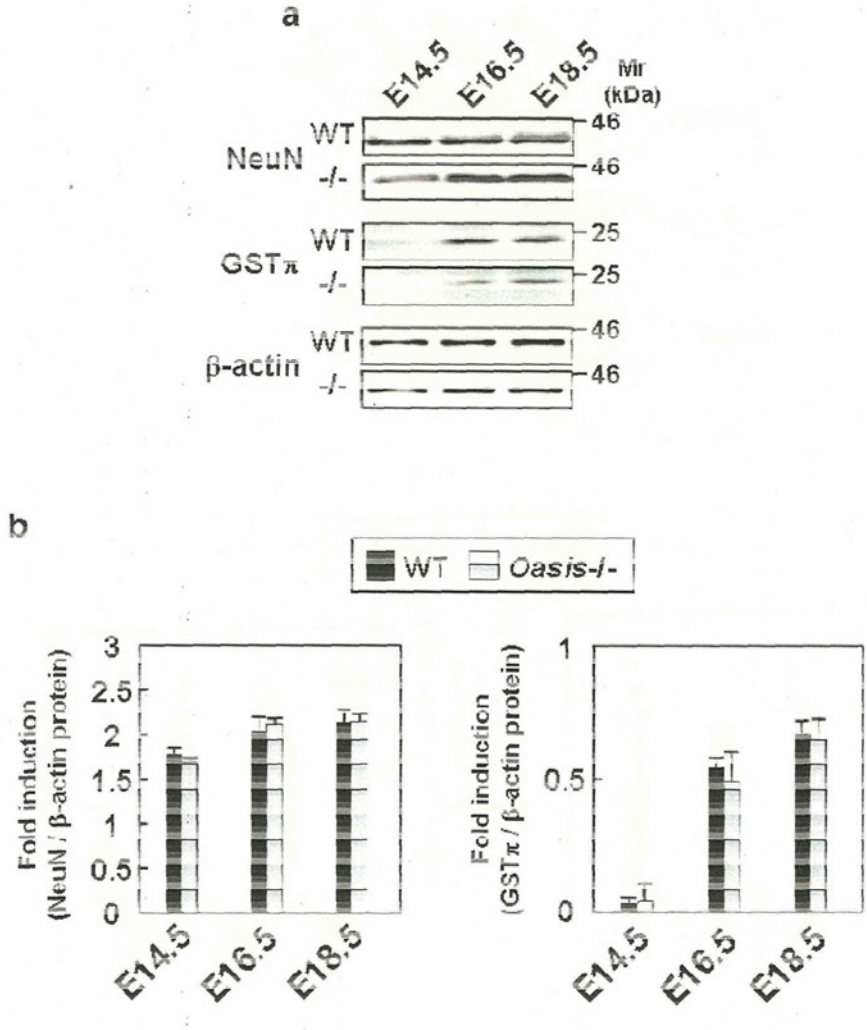

Supplementary Figure S2. *Oasis* deficiency does not affect the differentiation of NPCs. (**a**) Western blotting of NeuN and GSTπ in the cerebral cortices of WT and *Oasis*$^{-/-}$ mice. NeuN, a neuronal marker, and GSTπ, an oligodendrocyte marker, expression levels were not affected by *Oasis* deficiency. (**b**) Quantitative analysis of protein expression levels in (**a**). All bars represent the mean values ±s.d. of 3 experiments.

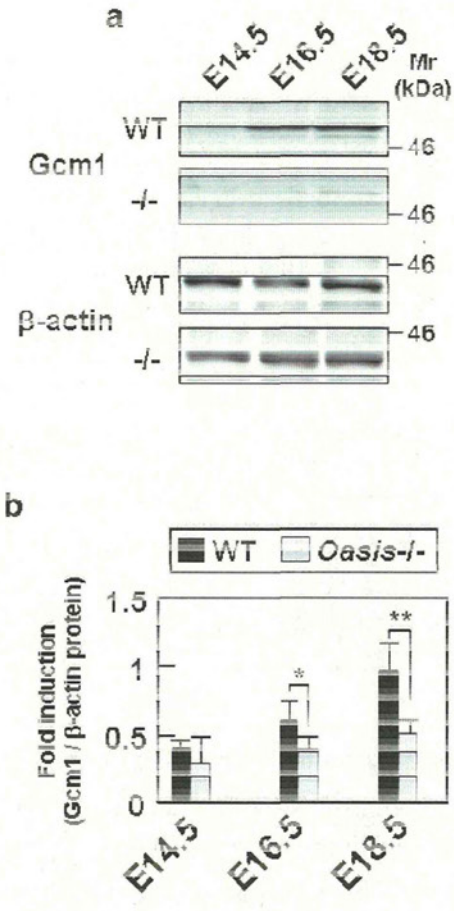

Supplementary Figure S3. Expression of Gcm1 is down-regulated in *Oasis*$^{-/-}$ mice. (**a**) Expression of Gcm1 was induced in the cerebral cortices of mouse embryos after embryonic day (E) 16.5. In *Oasis*$^{-/-}$ mice, it was inhibited compared with that in WT mice. (**b**) Quantitative analysis of Gcm1 expression in (**a**). All bars represent the mean values ±s.d. of 3 experiments. Significant difference was determined by unpaired Student's-*t*-test. $*P < 0.05$, $**P < 0.01$, between indicated pairs.

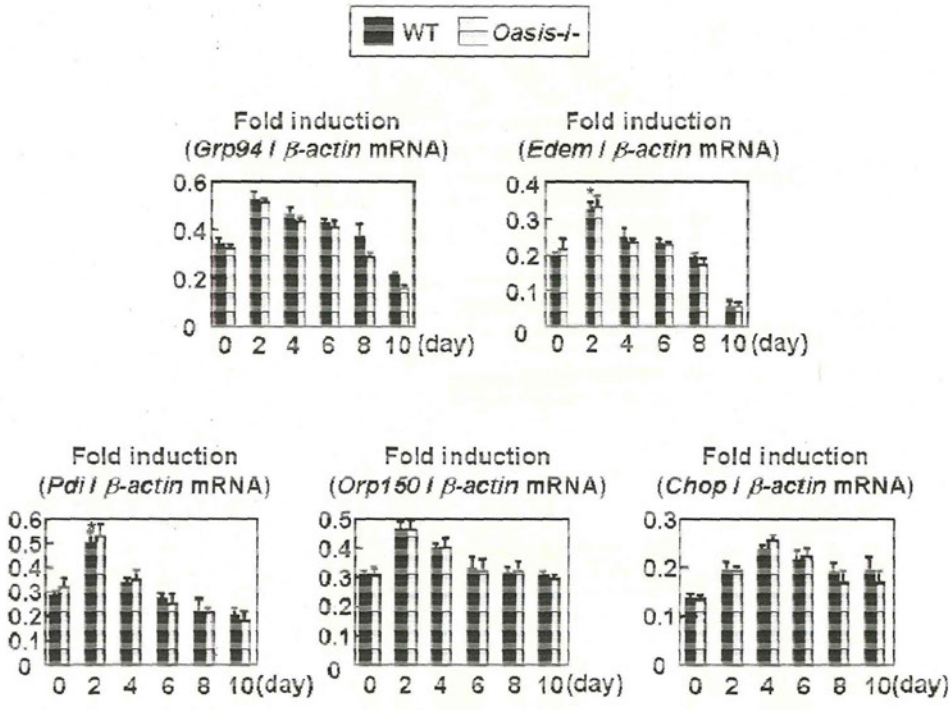

Supplementary Figure S4. ER stress occurs during astrocyte differentiation. Real-time PCR analysis of ER stress-related genes in primary cultured neural precursor cells (NPCs) treated with LIF and BMP2 for the indicated times. Mild ER stress transiently occurred (from day 2 to day 6) during the differentiation of NPCs into astrocytes. All bars represent the mean values ±s.d. of 4 experiments. Significant difference was determined by One way ANOVA followed by Tukey's post hoc test. $*P < 0.05$, among WT cells.

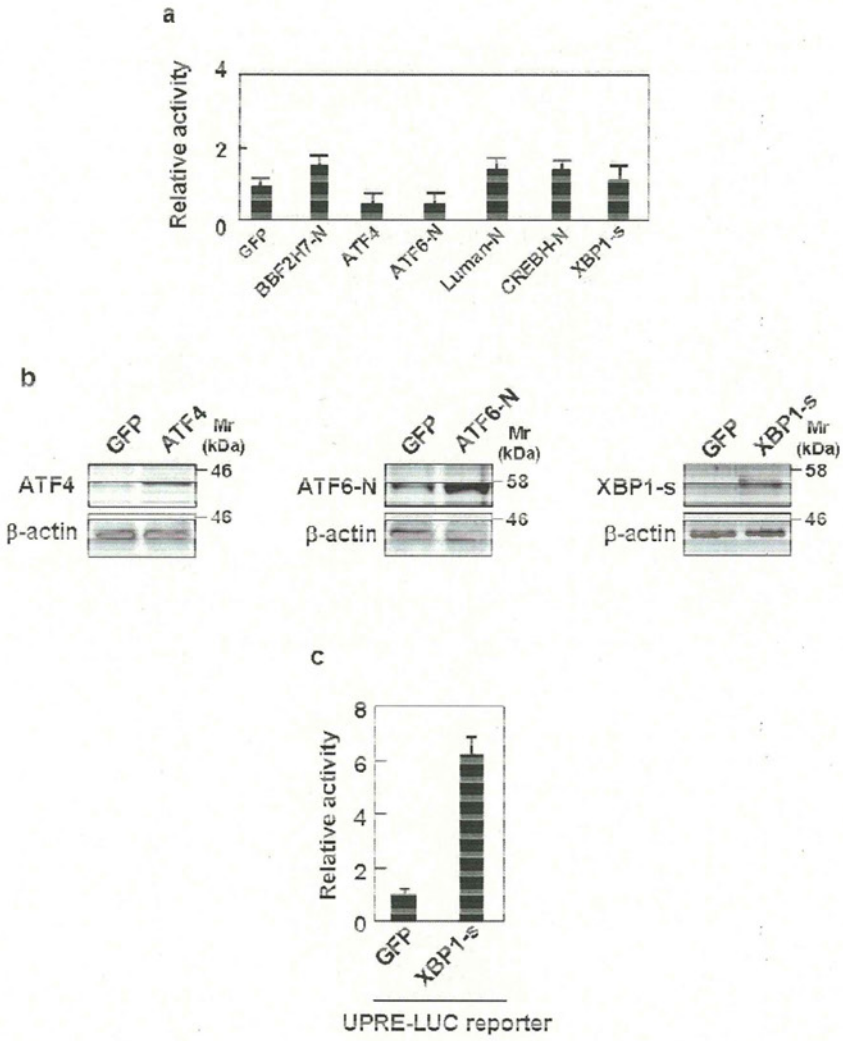

Supplementary Figure S5. Other CREB/ATF family members don't affect *Gcm1* promoter activation. (**a**) Reporter assays using NPCs. Vectors expressing the N-termini of mouse BBF2H7, ATF6, Luman and CREBH and the spliced form of XBP1 (XBP1-s), ATF4, and green fluorescent protein (GFP) were co-transfected with each *Gcm1*-Luc construct. GFP was used as a control. N: N-terminus. (**b**) Western blotting analysis in NPCs transfected with each expression plasmid. (**c**) Reporter assays using NPCs. Vectors expressing the XBP1-s was co-transfected with UPRE-LUC reporter. All bars represent the mean values ±s.d. of 3 (**a**) and 2 (**c**) experiments.

Gene name	accession number	position of complementary DNA
Oasis	NM_011957.2	nucleotides 66 to 1184
Bbf2h7	NM_178661.3	nucleotides 340 to 1470
Atf6	NM_001081304.1	nucleotides 71 to 1165
Luman	NM_013497.3	nucleotides 180 to 893
Crebh	NM_145365.3	nucleotides 422 to 1372
Creb4	NM_030080.2	nucleotides 210 to 1022
Xbp1	NM_013842.2	nucleotides 29 to 506, 533 to 1170
Atf4	NM_009716.2	nucleotides 595 to 1644

Supplementary Table S1. National Center for Biotechnology Information's accession numbers and the positions of complementary DNAs inserted into the plasmids.

Gene name	Sense primer (5' - 3')	Antisense primer (5' - 3')
Gfap	GCAGATGAAGCCACCCTGGCTC	CCAGATCGCAGGTCAAGGCCTGCAG
Nestin	CTACCAGGAGCGCGTGGC	TCCACAGCCAGCTGGAACTT
Bip	GTTTGCTGAGGAAGACAAAAAGCTC	CACTTCCATAGAGTTTGCTGATAATTG
P58^{IPK}	GAGGTTTGTGTTTGGGATGCAG	GCTCTTCAGCTGACTCAATCAG
Grp94	GCCGAGAAGGCTCAAGGACAG	CACCCGTGTCTGTGACATGCAG
Erdj4	CCCCAGTGTCAAACTGTACCAG	AGCGTTTCCAATTTTCCATAAATT
Edem	AAGCCCTCTGGAACTTGCG	AACCCAATGGCCTGTCTGG
Pdi	CAAGATCAAGCCCCACCTGAT	AGTTCGCCCCAACCAGTACTT
Orp150	GATGTCTGTAGACCTGGGCAGTG	GAACTGCAGCTGCGGACTGATCTG
Chop	GTCCAGCTGGGAGCTGGAAG	CTGACTGGAATCTGGAGAG
Xbp1	ACACGCTTGGGAATGGACAC	CCATGGGAAGATGTTCTGGG
β-actin	TCCTCCCTGGAGAAGAGCTA	TCCTGCTTGCTGATCCACAT

Supplementary Table S2. The primer sets used for real-time PCR and RT-PCR.

STEM CELLS®
REGENERATIVE MEDICINE

Treatment of a Mouse Model of Spinal Cord Injury by Transplantation of Human Induced Pluripotent Stem Cell-Derived Long-Term Self-Renewing Neuroepithelial-Like Stem Cells

YUSUKE FUJIMOTO,[a,b] MASAHIKO ABEMATSU,[b] ANNA FALK,[c] KEITA TSUJIMURA,[a] TSUKASA SANOSAKA,[a] BERRY JULIANDI,[a,d] KATSUNORI SEMI,[a] MASAKAZU NAMIHIRA,[a] SETSURO KOMIYA,[b] AUSTIN SMITH,[c] KINICHI NAKASHIMA[a]

[a]Laboratory of Molecular Neuroscience, Graduate School of Biological Sciences, Nara Institute of Science and Technology, Ikoma, Japan; [b]Department of Orthopaedic Surgery, Graduate School of Medical and Dental Sciences, Kagoshima University, Kagoshima, Japan; [c]Department of Biochemistry, Wellcome Trust Centre for Stem Cell Research, Stem Cell Institute, University of Cambridge, Cambridge, United Kingdom; [d]Department of Biology, Bogor Agricultural University (IPB), Bogor, Indonesia

Key Words. Spinal cord injury • Induced pluripotent stem cells • Neural stem cells • Transplantation • Regenerative medicine

ABSTRACT

Because of their ability to self-renew, to differentiate into multiple lineages, and to migrate toward a damaged site, neural stem cells (NSCs), which can be derived from various sources such as fetal tissues and embryonic stem cells, are currently considered to be promising components of cell replacement strategies aimed at treating injuries of the central nervous system, including the spinal cord. Despite their efficiency in promoting functional recovery, these NSCs are not homogeneous and possess variable characteristics depending on their derivation protocols. The advent of induced pluripotent stem (iPS) cells has provided new prospects for regenerative medicine. We used a recently developed robust and stable protocol for the generation of long-term, self-renewing, neuroepithelial-like stem cells from human iPS cells (hiPS-lt-NES cells), which can provide a homogeneous and well-defined population of NSCs for standardized analysis. Here, we show that transplanted hiPS-lt-NES cells differentiate into neural lineages in the mouse model of spinal cord injury (SCI) and promote functional recovery of hind limb motor function. Furthermore, using two different neuronal tracers and ablation of the transplanted cells, we revealed that transplanted hiPS-lt-NES cell-derived neurons, together with the surviving endogenous neurons, contributed to restored motor function. Both types of neurons reconstructed the corticospinal tract by forming synaptic connections and integrating neuronal circuits. Our findings indicate that hiPS-lt-NES transplantation represents a promising avenue for effective cell-based treatment of SCI. STEM CELLS *2012;30:1163–1173*

Disclosure of potential conflicts of interest is found at the end of this article.

INTRODUCTION

Our current ability to reconstruct the damaged central nervous system, including spinal cord injury (SCI), is limited. SCI is one of the commonest causes of loss of movement and sensation below the level of the injured spinal cord. While partial spontaneous functional recovery has been observed in the case of moderate SCI, there is no adequate treatment to repair the injured spinal cord itself, and most patients have no therapeutic options except for general management and rehabilitation [1].

Transplantation of neural stem cells (NSCs) into the injured spinal cord has been shown to be an effective treatment [2] because of their competence to differentiate into neurons and oligodendrocytes and to secrete neurotrophic factors. Transplantation into injured spinal cords of several different types of human NS/progenitor cells, derived from human fetal tissue [3, 4] or from human embryonic stem cells (hESCs) [5, 6], promotes functional recovery in animal models. Nonetheless, the mechanism underlying such functional improvement remains to be fully elucidated.

The establishment of induced pluripotent stem cells (iPSCs) offers new prospects for regenerative therapies [7, 8]. Human iPSCs (hiPSCs) can be generated from cells in adult tissue, making it possible to create iPSCs from SCI patients themselves. From the viewpoint of ethics and host immune rejection, NSCs derived from human iPSCs (hiPS-NSCs)

Author contributions: Y.F.: conception and design, collection and assembly of data, data analysis and interpretation, and manuscript writing; A.F. and A.S.: provision of study materials; M.A., K.T., T.S., K.S., and M.N.: collection and assembly of data, data analysis and interpretation; B.J.: manuscript writing; S.K.: administrative support; K.N.: conception and design, administrative support, manuscript writing, and final approval of manuscript.

Correspondence: Kinichi Nakashima, Ph.D., Laboratory of Molecular Neuroscience, Graduate School of Biological Sciences, Nara Institute of Science and Technology, 8916-5 Takayama, Ikoma 631-0192, Japan. Telephone: 81-743-72-5471; Fax: 81-743-72-5479; e-mail: kin@bs.naist.jp. Received October 18, 2011; accepted for publication February 11, 2012; first published online in STEM CELLS *EXPRESS* March 14, 2012. 1066-5099/2012/$30.00/0 doi: 10.1002/stem.1083

appear to be an ideal resource for transplantation therapy, and the efficacy of hiPS-NSC transplantation in SCI treatment has just begun to be investigated using the mouse model of SCI [9].

We used a recently developed protocol for the generation of long-term self-renewing neuroepithelial-like stem (lt-NES) cells, which satisfy the criteria to be defined as NSCs, from several different lines of hESCs and hiPSCs [10, 11]. hiPSC-derived lt-NES (hiPS-lt-NES) cells exhibit consistent characteristics such as continuous expandability, stable neuronal and glial differentiation ability, and the capacity to generate functional mature neurons in monolayer culture. Whereas neurosphere cultures display heterogeneous character and are sensitive to variation in methodological procedures [12], monolayer cultures offer a more homogeneous and robust cell generation [13, 14].

We report here that transplanted hiPS-lt-NES cells, derived from our robust and stable monolayer cultures, have a therapeutic potential comparable to that of NSCs from human fetal spinal cord (hsp-NSCs) for SCI in the nonobese diabetic-severe combined immunodeficient (NOD-SCID) mouse model. We further show that hiPS-lt-NES cell transplantation promotes recovery of hind limb motor function through the reconstruction of the corticospinal tract (CST), and restores disrupted neuronal circuitry in a relay manner as we have previously demonstrated in a study of mouse NSC transplantation [15]. Our results suggest that hiPS-lt-NES cells represent a promising cell source for transplantation into the injured spinal cord.

Materials and Methods

Cell Culture

hsp-NSCs and hiPS-lt-NES cells were established and maintained as described previously [10, 11, 16]. The hsp-NS cell line CB660sp and hiPS-lt-NES cell line AF22 were used in the present study. hsp-NSCs were plated onto 10 μg/ml laminin (Sigma, St. Louis, MO, http://www.sigmaaldrich.com)-coated plates in maintenance medium, consisting of Euromed-N medium (Euroclone, Milano, Italy, http://www.euroclonegroup.it), 2 mM L-glutamine, 0.1 mg/ml penicillin/streptomycin (Sigma), N2 supplement (1:100), 20 ml/l B27 (all from Invitrogen, Carlsbad, CA, http://www.invitrogen.com), 10 ng/ml fibroblast growth factor (FGF, R&D Systems, Minneapolis, MN, http://www.rndsystems.com)-2, and 10 ng/ml epidermal growth factor (EGF, R&D Systems). Cells were passaged at a ratio of 1:2 every second to third day using Accutase (Sigma). hiPS-lt-NES cells were plated onto 0.1 mg/ml poly-L-ornithine and 10 μg/ml laminin (O/L, Sigma)-coated plates in maintenance medium, consisting of Dulbecco's modified Eagle's medium/F12 (Invitrogen), 2 mM L-glutamine, 1.6 mg/ml glucose, 0.1 mg/ml penicillin/streptomycin, N2 supplement (1:100), 1 μl/ml B27, 10 ng/ml FGF2 and 10 ng/ml EGF. Cells were passaged at a ratio of 1:3 every second to third day using trypsin. To induce in vitro differentiation, hiPS-lt-NES cells were plated onto an O/L-coated 35-mm dish at a density of 5×10^5 cells per dish in culture medium without both EGF and FGF, containing 1% fetal bovine serum (FBS), and cultured for 4 weeks. Half of the medium was changed every 2 days and laminin (1:500) was added to the medium once a week to prevent detachment of the cells.

Lentivirus Production and Infection of hsp-NSCs and hiPS-Lt-NES Cells

Lentivirus production and infection of cells were performed as described previously [17, 18]. hsp-NSCs and hiPS-lt-NES cells were infected with lentiviruses harboring the luciferase and green fluorescent protein (GFP) genes connected by an internal ribosomal entry site (IRES), EFp (elongation factor promoter)-luciferase-IRES-GFP (Fig. 1B). hsp-NSCs and hiPS-lt-NES cells that had undergone more than 20 passages were infected. GFP-positive cells were collected by fluorescence activated cell sorting (FACS)-Aria II CellSorter (B.D. Biosciences, San Jose, CA, http://www.bdbiosciences.com) and used for transplantation.

SCI Model and Cell Transplantation

All aspects of animal care and treatment were carried out according to the guidelines of the experimental animal care committee of Nara Institute of Science and Technology. We used female NOD-SCID mice (8-10 weeks old, weighing 18-20 g, Charles River, Osaka, Japan, http://www.crj.co.jp). Anesthetized (ketamine 50 mg/kg, xylazine 5 mg/kg, and sodium pentobarbital 20 mg/kg) mice received laminectomies and partial laminectomies at the ninth and 10th thoracic spinal vertebrae, respectively. The dorsal surface of the dura mater was exposed and SCI was induced using an SCI device (70 kdyn; Infinite Horizon impactor, Precision Systems & Instrumentation, Lexington, KY, http://www.presysin.com) as previously described [15]. The muscle and skin were closed in layers. All mice subcutaneously received gentamicin (8 mg/kg) daily. The mice underwent manual bladder evacuation once a day. Seven days after injury, mice were anesthetized and transplanted with hiPS-lt-NES cells or hsp-NSCs using a glass micropipette attached to a stereotaxic injector (Narishige, Tokyo, Japan, http://www.narishige.co.jp). The tip of the micropipette was inserted into the injury epicenter in the injured spinal cord, and 2 μl of culture medium lacking growth factors, with or without NSCs (5×10^5 μl^{-1}), was injected at a rate of 1 μl/min.

Behavioral Testing and Electrophysiological Recordings

We evaluated the motor function of the hind limbs for up to 10 weeks after injury. Two individuals, blinded to the treatment of the mice, examined motor function using the Basso Mouse Scale (BMS) locomotor rating scale [19]. Hind limb movements of the mice were captured using a high-definition digital camcorder. We edited these movies and exported movie files using editing software.

To examine signal conduction in motor pathways after SCI, motor-evoked potentials (MEPs) at 12 weeks after SCI were measured. Mice were anesthetized with intraperitoneally injected ketamine (100 mg/kg) and their heads were fixed in a stereotactic frame. The skulls were tightly fixed to a stereotaxic apparatus (Narishige). Scalping and two small craniotomies were performed with a drill over the motor cortex area (Nakanishi, Tochigi, Japan; http://www.nsk-nakanishi.co.jp). Silver ball electrodes were placed epidurally via the holes, into which mineral oil was applied. The motor cortex was stimulated with 0.2-msecond square wave pulses at a constant current of 10 mA using an electrical stimulator (SEM-3301, Nihon Kohden, Tokyo, Japan; http://www.nihonkohden.co.jp). Recording needle electrodes were inserted into the hamstring. A subcutaneous ground electrode was placed in the tail. Electrophysiological recordings were made (MED64, Alpha MED Scientific, Osaka, Japan; http://www.amedsci.com) and band-pass filtered at 1-10 kHz. Amplitudes from onset to peak of the negative deflection were measured. Latency of MEP was measured as the time interval between the end of stimulation and the onset of the first wave. Indicated values are the average of five experiments from each mouse.

Antibodies

The following antibodies were used: rabbit anti-Sox2 (1:1,000, Chemicon-Millipore, Billerica, MA, http://www.millipore.com), mouse anti-Nestin (1:250, Chemicon), rabbit anti-brain lipid-binding protein (BLBP, 1:500, Abcam, Cambridge, U.K., http://www.abcam.com), mouse anti-β-tubulin isotype III (Tuj1; 1:500,

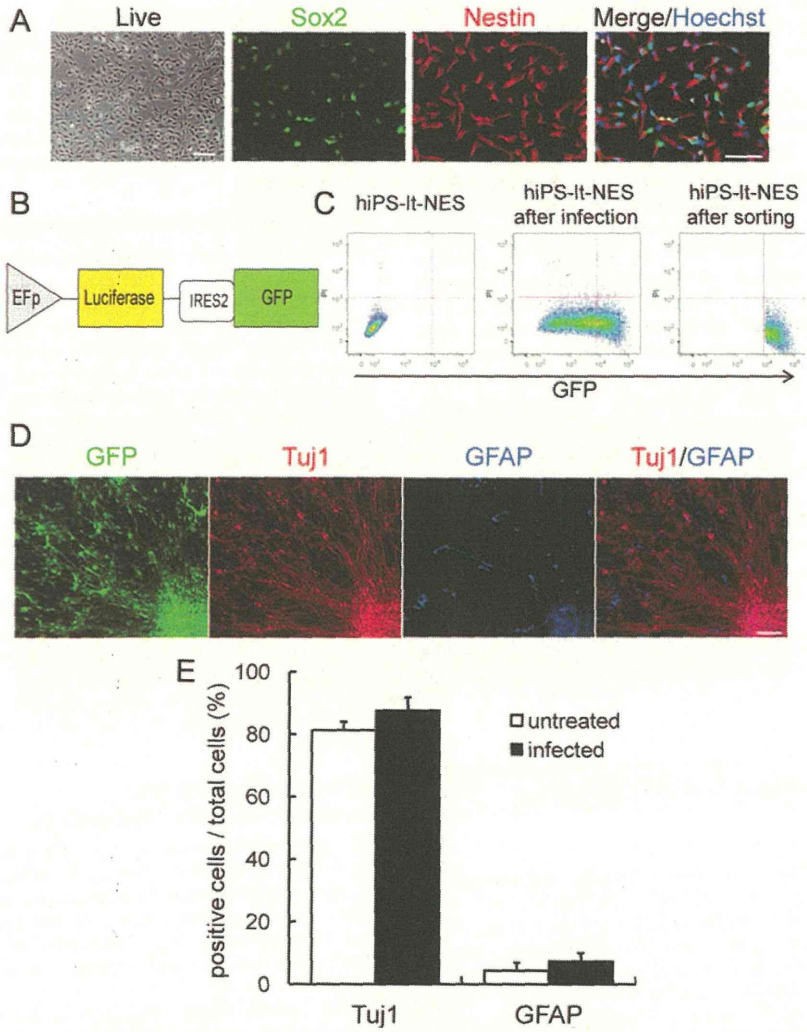

Figure 1. Characterization of hiPS-lt-NES cells. **(A):** Expansion culture. hiPS-lt-NES cells can be expanded continuously in the presence of both epidermal growth factor and fibroblast growth factor. hiPS-lt-NES cells were uniformly immunopositive for Sox2 (green) and Nestin (red). Hoechst (blue) shows nuclear staining. **(B):** The pCSII-EFp-luciferase-IRES2-GFP construct. **(C):** Flow cytometric analysis of GFP-positive cells in hiPS-lt-NES cells. Uninfected cells (left) and cells infected with lentiviruses expressing luciferase and GFP (middle) were subjected to flow cytometric analysis. GFP-positive cells in the infected cell population were sorted on the basis of GFP fluorescence and reanalyzed for GFP expression (right). **(D):** After 4 weeks in differentiation conditions, infected hiPS-lt-NES cells differentiated into Tuj1-positive neurons (red) and GFAP-positive astrocytes (blue). **(E):** Quantification of neural marker-positive cells after 4 weeks' differentiation. Lentiviral infection did not influence the differentiation tendency. Data are means ± SD ($n = 3$). Scale bars = 100 μm. Abbreviations: EFp, elongation factor promoter; GFP, green fluorescent protein; GFAP, glial fibrillary acidic protein; hiPS-lt-NES, human induced pluripotent stem cell-derived long-term self-renewing neuroepithelial-like stem; and IRES2, internal ribosomal entry site 2.

Sigma), rabbit anti-β-tubulin isotype III (Tuj1; 1:1,000, Covance, Madison, WI, http://www.covance.com), rabbit anti-GFP (1:1,000, Molecular Probes, Carlsbad, CA, http://probes.invitrogen.com), chick anti-GFP (1:500, Aves Labs, Tigard, OR, http://www.aveslab.com), rabbit anti-glial fibrillary acidic protein (GFAP, 1:2,000, DAKO, Carpinteria, CA, http://www.dako.com), mouse anti-human-specific GFAP (hGFAP, 1:1,000, STEM123, StemCells Science, Newark, CA, http://www.stemcellsinc.com), mouse anti-MAP2ab (1:500, Sigma), chick anti-myelin basic protein (MBP) (1:200, Aves Labs), mouse anti-adenomatous polyposis coli CC-1 (APC, 1:200, Calbiochem-Merck, Darmstadt, Germany, http://www.merckgroup.com), mouse anti-synaptophysin (1:200, Chemicon), mouse anti-Bassoon (Bsn, 1:400, Stressgen-Enzo Life Sciences, Plymouth Meeting, PA, http://www.enzolifesciences.com), mouse anti-human-specific synaptophysin (hSyn, 1:200, Chemicon), and mouse anti-NeuN (1:500, Millipore).

Immunocytochemistry

Immunocytochemistry experiments were performed as described previously [20]. Cells were washed with phosphate buffered saline (PBS) and fixed with 4% paraformaldehyde (PFA) in PBS for 10 minutes, and then washed with PBS and incubated in blocking solution (PBS containing 10% FBS and 0.1% Triton X-100). Subsequently, cells were incubated overnight at 4°C with the primary antibodies described above. After three washes in PBS, cells were incubated for 1 hour with the following secondary antibodies: FITC-conjugated donkey anti-chick/rabbit, Cy3-

conjugated donkey anti-chick/mouse/rabbit, Cy5-conjugated donkey anti-mouse/rabbit (1:500, Jackson ImmunoResearch, West Grove, PA, http://www.jacksonimmuno.com). After three washes with PBS, nuclei were stained with Hoechst (bisbenzimide H33258 fluorochrome trihydrochloride, Calbiochem-Merck). Samples were washed with PBS and mounted on glass slides with Immu-Mount (Thermo Scientific, Waltham, MA, http://www.thermoscientific.com). The cells were examined using a fluorescence microscope (Axiovert 200M, Zeiss, Jena, Germany, http://www.zeiss.com) equipped with the appropriate epifluorescence filters.

Immunohistochemistry

Animals were anesthetized and perfused with PBS followed by 4% PFA in 0.1 M PBS, pH 7.4. The spinal cords were dissected and postfixed overnight in the same fixative at 4°C. For cryosectioning, fixed tissues were cryoprotected in 10% sucrose in PBS overnight at 4°C, then in 20% sucrose in PBS overnight at 4°C, and embedded in optimal cutting temperature (OCT) compound (Tissue Tek, Sakura Finetek, Tokyo, Japan, http://www.sakura-finetek.com). Cryostat sections (20 μm) were cut and affixed to matsunami adhesive slide (MAS)-coated glass slides (Matsunami Glass, Osaka, Japan, http://www.matsunami-glass.co.jp). The sections were permeabilized in PBS-T (PBS containing 0.1% Triton X-100) for 10 minutes and blocked with 10% FBS in PBS-T for 1 hour, and then incubated overnight at 4°C with the primary antibodies described above. After three washes with PBS, they were incubated in a mixture of the secondary antibodies described above for 1 hour. After a final rinse with PBS, nuclei were stained using Hoechst. Sections were mounted and examined under a fluorescence microscope (Axiovert 200M, Zeiss) and a scanning laser confocal imaging system (LSM 710, Zeiss).

In Vivo Imaging of Transplanted Cells

In vivo imaging experiments were performed as described previously [18]. A Xenogen-IVIS 100 cooled CCD optical macroscopic imaging system (SC BioScience, Tokyo, Japan, www.scbio.co.jp) was used for bioluminescence imaging. Mice were given an intraperitoneal injection of D-luciferin (150 mg/kg) and serial images were acquired from 20 minutes after administration until the maximum intensity was obtained with the field-of-view set at 10 cm. All images were analyzed using Igor (WaveMetrics, Portland, OR, http://www.wavemetrics.com) and Xenogen Living Image software, and optical signal intensity was expressed as photon flux in units of photons/s per cm^2/steradian. To quantify the measured light, we defined regions of interest (ROIs) over the cell-implanted area and examined all values within the same ROI. The obtained photon count intensity was expressed as a percentage of the initial value.

Anterograde Labeling of the CST

Twelve weeks after injury, descending CST fibers were labeled with biotinylated dextran amine (BDA) (MW 10,000, 10% in saline, 2 μl per cortex; Molecular Probes) [21, 22] by injection into the left and right motor cortices [23]. The skulls of anesthetized mice were tightly fixed to a stereotaxic apparatus (Narishige). Scalping and craniotomy over the motor cortex area were carried out using a micromotor system (Nakanishi). The injection site was 2.1 mm posterior to the bregma, 2 mm lateral to the bregma, and 0.7 mm in depth [23]. For pressure injections with a 20-μm outer diameter glass capillary attached to a microsyringe (Narishige), we used 0.1-μl steps per minute until the desired volume (1 μl per injection site) was injected. Two weeks later, the animals were perfused and their spinal cords were fixed as described above. Sections (30 μm) were cut and used for immunohistochemistry. To visualize the BDA, a tyramide signal amplification fluorescence system (Perkin Elmer, Waltham, MA, http://www.perkinelmer.com) was used.

Visualization of Multisynaptic Neural Pathways

To visualize selective and functional transsynaptic neural pathways, wheat germ agglutinin (WGA)-expressing recombinant adenoviruses were used [24, 25]. Twelve weeks after injury, 1 μl of saline containing WGA-expressing virus at a titer of 1×10^{11} pfu/ml was injected into the bilateral motor cortices (0.5 μl per injection site). The injection site was 2.1 mm posterior to the bregma, 2 mm lateral to the bregma, and 0.7 mm in depth. Two weeks later, animals were perfused and the spinal cords were fixed as described above. Sections (15 μm) were cut and used for immunohistochemistry. Rabbit anti-WGA polyclonal antibody (3 μg/ml, Sigma) was preabsorbed with 1% acetone powder of mouse brains in blocking solution overnight at 4°C.

Ablation of Transplant-Derived Cells

Cell ablation experiments were performed as described previously [26, 27]. Diphtheria toxin (DT) was purified from conditioned medium of the PW8 strain of *Corynebacterium diphtheriae* by diethylaminoethyl Sepharose column chromatography and diluted to an appropriate concentration with saline. Seven weeks after injury, DT solution (50 μg/kg per day $\times$ 2 days) was administered by intraperitoneal injection into seven hiPS-NES cell-transplanted mice.

Statistical Analysis

We performed statistical analysis with an unpaired two-tailed Student's t test for single comparisons. For &&&BMS and BDA fiber analysis, we used repeated-measures analysis of variance (ANOVA) with Tukey-Kramer multiple comparison test at each point (Prism, GraphPad, LA Jolla, CA, http://www.graphpad.com). $p < .05$ was considered significant.

Results

Characterization of hiPS-Lt-NES Cells In Vitro

We have previously shown that hiPS-NES cells, which are reliably derived from different hiPS cell lines, exhibit consistent characteristics such as continuous expandability, stable neuronal and glial differentiation, and the capacity to generate functional mature human neurons [11]. hiPS-lt-NES cells can be expanded in the presence of FGF2 and EGF in monolayer culture, and express the NSC markers Sox2 and Nestin (Fig. 1A) and the radial glial marker BLBP (Supporting Information Fig. 1), but not the ES/iPS cell markers Oct3/4 or Nanog (not shown).

To visualize transplanted cells by both luminescence and fluorescence, hiPS-lt-NES cells were infected with lentiviruses engineered to express luciferase and GFP (Fig. 1B). Almost all hiPS-lt-NES cells were infected (Fig. 1C, middle), and we isolated only strongly GFP-expressing cells for use in subsequent in vitro and transplantation experiments (Fig. 1C, right).

We then examined whether lentiviral infection affected the differentiation potential of hiPS-lt-NES cells. Uninfected and infected hiPS-lt-NES cells were induced to differentiate by removal of growth factors and cultured in the presence of 1% FBS for 4 weeks. Both hiPS-lt-NES cell population differentiated into large and small numbers of Tuj1-positive neurons and GFAP-positive astrocytes, respectively, as observed in our previous study [11] (Fig. 1D). Quantitative analysis revealed no significant differences in the proportions of differentiated cells between uninfected and infected hiPS-lt-NES cells (Fig. 1E). Thus, we concluded that lentiviral infection did not influence the differentiation potential of hiPS-NES cells.